CUIMR-T-86-003 C2

WAVE INDUCED SEABED EFFECTIVE STRESS DISTRIBUTION INCLUDING ROTATIONAL SHEAR EFFECT

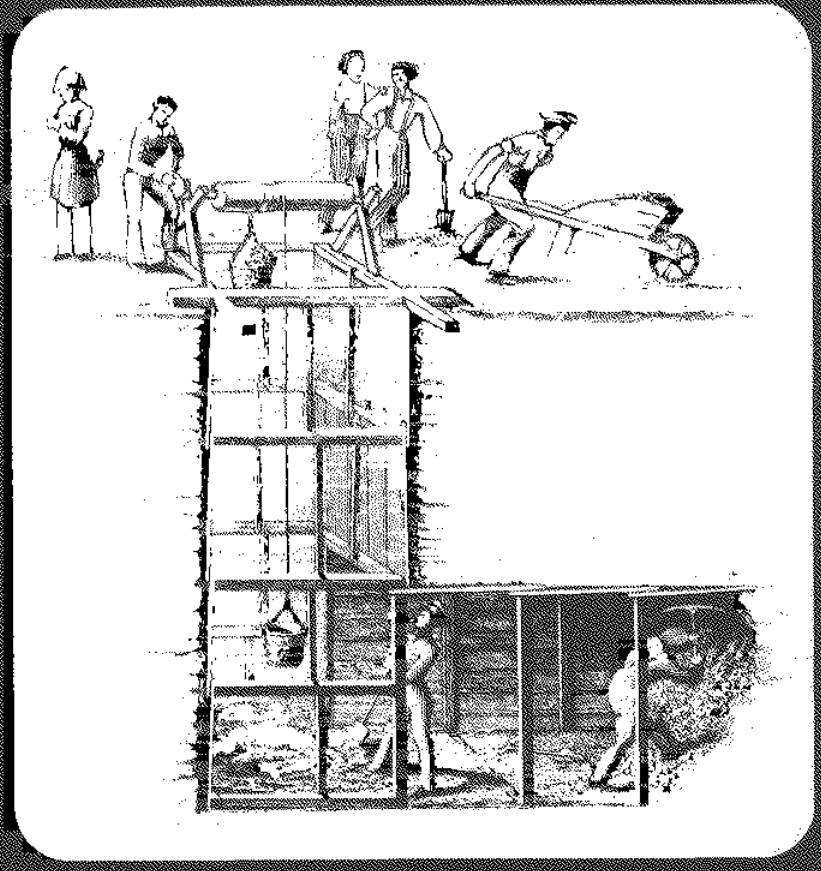

Department of Civil Engineering

University of California, Davis

FINAL REPORT
ON
OCEAN WAVE INDUCED EFFECTIVE STRESSES IN AN ELASTOPLASTIC SEAFLOOR

FOR

The California Sea Grant College Program
Project Number R/OT-13

Prepared by

C.K. Shen
Z.L. Wang
L.R. Herrmann

Department of Civil Engineering
University of California, Davis

November 1986

WAVE INDUCED SEABED EFFECTIVE STRESS DISTRIBUTION INCLUDING ROTATIONAL SHEAR EFFECT

SUMMARY

The stability of a seabed under wave action has been the subject of a number of recent studies. Among them are theoretical analyses using elastic or visco-elastic soil models, laboratory investigations of soil under rotational shear loading and wave tank experiments of soil deposits under wave loading. Discrepancies seem to exist between available analytical predictions and experimental results.

It is generally agreed that the inclusion of the effects of rotational shear loading induced by traveling waves is essential in studying the seabed response to wave loading. This paper offers a theoretical approach for analyzing stability of wave loaded seabeds by incorporating the recently developed bounding surface plasticity model for sandy soils into a general two dimensional finite element program "SAC2". Since the plasticity model can adequately describe the generation of pore water pressure under different cyclic stress paths in a multi-dimensional stress space, a more realistic prediction of wave induced seabed soil response is therefore achievable.

An example of a wave loaded deep loose sand deposit was analyzed using the "SAC2" program and the plasticity soil model. The results were compared with numerical solutions for an elastic medium. Furthermore, failure criteria for soils were discussed to aid in defining stable or unstable conditions for seabed deposits.

Finally, a comparison between a wave tank experiment and theoretical predictions using both elastic and plastic soil properties is presented. The effective stresses and pore water pressure distributions predicted

by the bounding surface plasticity model solution are closer to the experiment results than those obtained from the elastic solution.

INTRODUCTION

The stability of the seafloor under wave action is an important consideration in the design of pipelines, anchors, and offshore structures such as gravity or pile supported platforms. The interaction of ocean waves and the seafloor is a very complex phenomenon. In order to simplify it, storm waves are almost invariably represented as a series of harmonic waves. These waves create dynamic pressure waves on the ocean floor, increasing the pressure under the crest and reducing it under the trough. The differential loading of the seafloor by the pressure waves create shear stresses in the underlying soil and, if they exceed the shear strength, significant deformation or an instability failure may result. A well documented case of wave-triggered instability of a seafloor during the passage of hurricane Camille (August, 1969) through the South Pass Block 70, in the Mississippi River Delta, was reported (1). A massive soil movement 3,000 feet wide extending to depths in excess of 90 feet was observed. Three offshore platforms failed as a result of the seafloor instability and the hurricane forces. Other events are evidenced by the flotation of buried pipelines on the Australian coast, and the uneven settlement of gravity-type oil drilling rigs in the North Sea.

The mathematical representation of the dynamic behavior of soil-fluid interaction in seafloor deposits due to ocean waves has been a topic of intensive study. The major differences among investigators are their selection of material models for the soil and whether pore water was treated as a separate phase or not. The seabed soil has been

considered to be presented by a variety of different material models such as rigid, elastic, visco-elastic, "viscous fluid" and "coulomb-friction" elastic body.

Putnam (18) assumed the sand skeleton to be incompressible, hydraulically isotropic, water flow to be governed by Darcy's law, and the seawater to be incompressible. Though his analysis neglects the mechanical properties of sand and the coupling of the sand skeleton and pore water in resisting waves, the simple, uncoupled solution has very wide applicability. Using Biot's equation (2) for poro-elastic solids, Yamamoto (22) and Madsen (16) have developed solutions for the effective stresses and transient pore water pressure in sand due to wave loading. A refinement of their solution can be found in a recent paper by Okusa (17). Later, in order to include damping effects, the seafloor was treated as an incompressible, viscous fluid by Gade (10), Dalrymple and Liu (6); and as an incompressible visco-elastic half space by Hsiao and Shemdin (14). The continuum approach by Hsiao and Shemdin disregards seepage flow and pore pressure development in the soil, thus no information is obtained concerning the effective stresses. In a recent publication, Yamamoto (25) presented a closed form solution for the response of a coulomb-damped medium to ocean waves.

In the solutions using elasticity or visco-elasticity soil models, the effective stresses resulting from harmonic wave loading are also harmonic functions of time. If this is true, the wave duration or wave cycles would not influence the solution. However, in reality, seafloor soil is not an elastic medium. Permanent deformation due to the wave loading is likely to take place. This will result in the development of residual pore water pressure in the seafloor soil that is not uniquely related to the instantaneous values of the wave-induced stresses, but

rather depends upon the plasticity of the soil, the intensity and duration of loading, and the drainage characteristics of the seafloor. Since storms may last for several hours or more, dissipation effects are very important and must be taken into account in order to obtain reliable estimates of residual pore water pressure.

Very little attention has been paid to the possible consideration of the seafloor as a plastic continuum. Seed and Rahman (19) have presented a procedure for estimating pore water pressure and liquefaction potential caused by cyclic shear stresses generated by a dynamic wave pressure varying harmonically in space and time. More recently, Finn, et al. (9) developed two computer programs for evaluating transient and residual pore water pressure. The computer program for residual pore water pressure is a generalization of the Seed-Rahman method, and includes the effects of the increasing pore water pressure on the shear and bulk moduli during a storm.

The cyclic shear strength and the buildup of pore water pressure in sand is generally estimated by laboratory cyclic triaxial compression and extension tests performed on "undisturbed" soil samples. However, Ishihara and Towhata (15) have shown recently that the shear stress history produced by waves for a seafloor deposit involves a continuous rotation of the principal stress directions under a constant deviatoric stress. Such stress histories unfortunately cannot be simulated in the conventional cyclic triaxial testing apparatus. A triaxial torsional shear test using a hollow cylindrical specimen was performed by Ishihara and Towhata to simulate actual stress conditions under wave loading. They found that for a constant amplitude of the combined deviatoric stress, plastic deformation, as represented by the buildup of pore water pressure for undrained conditions, could take place in sand.

Furthermore, if rotation of the principal stress axes occurs during the course of a cyclic loading test, the cyclic strength of sand is reduced in comparison with the cyclic strength determined from a conventional cyclic triaxial test. The above observation may raise some concern as to whether the current laboratory testing procedure is adequate for characterizing the field response of a soil subjected to wave loading. The effect of rotation of principal stress axes on the behavior of soils is a current research topic in experimental soil mechanics. Such stress states may well be encountered in foundations of off-shore structures where waves may produce complicated loading patterns in the seafloor soils.

A number of case studies and laboratory model studies have been reported (3,9,24) which compare measured and predicted transient pore water pressures in relatively shallow waters. For instance, Yamamoto (24) reported good agreement between pore pressures predicted by the poro-elastic analysis and those measured in situ in a fine-grained sediment bed in the Mississippi Delta area. Similar agreement was found by Finn, et al. for pore pressures recorded under field conditions in the Pacific Ocean (9) and those predicted using their computer program based on Biot's equations. However, a very recent wave tank study conducted at Cornell by Clukey, et al. (3) indicates that, overall, the effective stresses and the pore water pressures predicted by the basic solution, as presented by Yamamoto, are not verified by experimental results. In short, experimental results are too limited at this time to warrant a definitive opinion concerning the validity of available theories in predicting pore pressures or effective stresses in sand due to wave loading. Because the subject area is relatively new and not fully

appreciated by the profession, residual pore water pressure measurements are not available at this time.

Our inability to properly characterize seafloor response to ocean waves stems from a lack of understanding of the interactive mechanism between the soil and the pore water for wave loading conditions. The Cornell model test results have revealed a number of very interesting points concerning experimental observations and the poro-elastic solution:

1. The pore water pressure response was less than that predicted by the theory for all wave periods studied.

2. The horizontal effective stresses generally were less than those predicted by the theory; the vertical effective stresses, however, were greater than those predicted by the theory for the upper part of the deposit, but they attenuated more rapidly with depth than the theoretical predictions.

The discrepancies can be argued to result from the inadequate mathematical modeling of soil behavior, i.e. the poro-elastic model does not take into consideration energy loss, deviatoric stress related volume change and the degradation of soil strength with pore pressure buildup. The coulomb-damped poro-elastic model later used by Yamamoto is similar to the equivalent visco-elastic model sometimes used in earthquake response analyses of soils; it does not yield permanent deformation. Consequently it yields no residual pore pressure buildup and no degradation of soil stiffness with loading cycles. Furthermore, "rotational shear" or "principal stress rotation" due to wave loading is not considered in the soil characterization. It seems clear that any further attempts to analyze wave induced effective stresses in seafloor deposits should adopt an elasto-plastic soil model capable of incorporating the

effects of rotational shear loading and deviatoric stress induced volume changes in the analysis.

OUTLINE OF A HYPOPLASTICITY MODEL FOR SANDY SOILS

A constitutive model for granular soil based on the concept of bounding surface plasticity has recently been developed by Wang, Dafalias and Shen (21). In its present form for isotropic material, the model is capable of predicting drained and undrained behavior of sand in a multiaxial stress space under both monotonic and cyclic loading, including rotational shear loading and principal stress rotation. A well construed theoretical model will enable one to study the behavior of sand for general loadings in a multidimensional stress space, thus it can significantly improve analytical capability for realistically assessing seafloor stability under wave-induced loading as well as the seismic response of granular soil deposits during earthquakes.

The two major novel features of the model are the flow rule for a deviatoric plastic strain increment, and the incremental equation for the rate of pore water pressure generation (or plastic volumetric strain). In each case, the determination of the plastic strain increment depends not only on the stress state and internal variables, as is done in modern plasticity, but also on the direction (not magnitude) of the stress increment. Such an incremental nonlinear plasticity formulation is called hypoplasticity by Dafalias (5). Good agreement was obtained when theoretical predictions were made with the model and compared with Yamada and Ishihara's true triaxial laboratory results (22). Readers are referred to References (20,21) for detailed information concerning the theory.

2-D FINITE ELEMENT ANALYSIS ("SAC2" PROGRAM) AND MODEL CODE ("SAND" SUBROUTINE)

A set of computer programs "EVAL" (one-element-calibration code), "SAC2" (plane strain analysis) and "SAC3" (three-dimensional analysis) have been developed by Herrmann, Mish and Kaliakin at U.C. Davis (11,12,13), for the finite element analysis of soil structures. They are limited to small deformations and displacements, and classical consolidation theory. The codes make use of the comprehensive bounding surface plasticity constitutive model for cohesive soils originated by Dafalias (4). This tool has been extensively used to solve boundary value problems for cohesive soils. Recently, an improved numerical algorithm for the evaluation of the bounding surface model for cohesive soil was developed by Herrmann et al. (13). In this numerical implementation of the constitutive model, the calculation of stress and strain increments is accomplished by global and local iterations and includes a sub-incrementing process. It is valid for input data of any combination of stress and strain increments.

Recently, the newly developed bounding surface hypoplasticity model for sandy soils (cohesionless soils) has been implemented into a numerical code, i.e. a one element analysis program "EVALS", which follows the logic and iteration procedure used in "EVAL" for cohesive soil by Herrmann et al. (13). Because of the incremental nonlinearity between the strain increment and the stress increment direction in a hypoplasticity formulation, the convergence of the iteration process was sometimes not rapid. In addition to the above mentioned iteration and sub-incrementing procedures used in "EVAL", a filter technique has been explored and adopted in the numerical code for sand to ensure convergence. The filter technique appears to be an efficient tool for the

numerical implementation of hypoplasticity type constitutive models when achieving convergence is a problem.

The subroutine "SAND", used in "EVALS" for the evaluation of the new soil model has also been incorporated into "SAC2", thus "SAC2" is now capable of modeling elastic behavior as well as the elastoplastic behavior of cohesive and cohesionless soils. The matrix for the increment stress-strain equations for sand is not symmetric due to the use of a non-associated flow rule; it is separated into symmetric and antisymmetric parts before return to the parent program SAC2, the antisymmetric part is included in the load matrix through the iteration process (7).

The governing equation in "SAC2" consist of Mass Conservation, Water Flow, Force Equilibrium and Strain-Effective Stress Relations. For details concerning "SAC2", the readers are referred to references (11,12).

NUMERICAL SOLUTION FOR EFFECTIVE STRESSES IN AN ELASTIC SEABED

An analytical solution for effective stresses in an elastic seabed has been presented by Yamamoto (23) and Madson (16) and refined by Okusa (17). Other analytical solutions dealing with a layered seabed are also available (24). The 2-D finite element program "SAC2" is capable of solving the above elasticity problems numerically, if the inertia of the soil and water are neglected. The resulting effective stresses will be compared with those obtained from the analytical solutions.

Fig. 1 shows a cross-section of a sinusoidal traveling wave of period T, length L and height H riding on the surface of a body of water of depth D. The set of parameters used in the elastic solution is given in Table 1. These parameters are chosen in reference to data obtained at an offshore location in the North Sea (17). The seabed is assumed to

be a homogeneous, elastic half space. In addition, the basic parameters of permeability k and Young's Modulus E are specified for Biot's equation. If linear wave theory is applied, then the wave pressure amplitude p_o on the mud line may be calculated from the formula,

$$p_o = \frac{\rho_\omega g H}{2 \cosh(2\pi D/L)} \tag{1}$$

TABLE 1. Parameters for an elastic loose sand deposit (refer to (17))

Water depth D: 20 m, Wave height H: 2.5 m, Wave period T: 15 s
Wave length L: 197.4 m, Bulk density: 1.5 t/m^3, Poisson's ratio: 0.3
Young's Modulus E: 1.31 x 10^4 kN/m^2, Permeability k: 9.8 x 10^{-4} m/s.

In the analysis only harmonic waves are considered; the seabed is assumed to be horizontal and a portion of length equal to the wave length L is considered. The behavior at the vertical boundaries are unknown; however, due to the harmonic nature of the traveling wave recurrent conditions at the two vertical boundaries exist, i.e.,

$$u(0,y) = u(L,y),\ v(0,y) = v(L,y),\ p(0,y) = p(L,y) \tag{2}$$

in which p is the pore water pressure and u and v are displacements along x and y directions, respectively. The option for a "travelling wave loading" condition has been built into the "SAC2" program in a discrete form.

The boundary conditions at the seabed surface are specified as

$$\sigma'_y = 0\ ,\quad \tau_{xy} = 0\ ,\quad p = p_o \exp\left(i(\lambda x - \omega t)\right)\ ,\quad \text{at } y = 0 \tag{3}$$

That is, the vertical effective stress is zero, the shear stress is negligibly small, and a harmonic pressure fluctuation exists. To locate

the bottom boundary of the seabed, reference is made to the elastic solution, where it has been found that the influence of wave loading in an infinitely deep seabed is insignificant at depths more than half of the wave length (L/2). On the other hand the peak value of the effective stress is found at a depth of about $L/2\pi$. On this basis, the boundary conditions of the seabed bottom are chosen as

$$u = 0,\ v = 0,\ p = 0,\ \text{at } y = -L \tag{4}$$

The finite element mesh is shown in Fig. 2, in which the LxL sand deposit is discretized by 144 rectangular elements. The nodes in the horizontal layers are equally spaced. In each of the 12 sand columns, the spacing ratio between the nodes is a constant (in this example, 0.8, from bottom to top). This unequal node spacing enables a better description of the stress distribution to be obtained near the seabed surface than when using equally spaced node points.

The numerical solution for an elastic seabed under a harmonic wave loading is presented in Figs. 3 to 5. Fig. 3 shows that the stress paths in the 12 layers (elements 1 to 12) are circular in the τ_{xy} vs. $(\sigma_x-\sigma_y)/2$ stress subspace. Fig. 4 shows the amplitudes of the effective stress and pore water pressure variations with depth. Good agreement between the numerical and analytical solutions (16,23) is observed. It is to be noted that at a given depth the stresses σ'_x, σ'_y and τ_{xy} all have the same amplitudes ($\sigma'_x = -\sigma'_y$) and they reach a maximum value of $0.35p_o$ at a depth of 0.18L (the analytical solution gives a maximum value of $0.36p_o$ at $L/2\pi = 0.16L$). The effective stress σ'_z is almost zero for both solutions. Fig. 5 shows the time history of the stresses in element 8 (the layer in which the harmonic stresses reach maximum

amplitudes). This example demonstrates the capability of the "SAC2" program in solving problem for harmonic wave loading.

In the following, a multi-layered elastic seabed is considered. The elastic modulus is assumed to be overburden dependent; that is, the deeper the layer, the larger the elastic modulus. An assumed distribution of Young's modulus E with depth is shown in Fig. 6 along with the constant Young's modulus E used above for the "homogeneous" elastic seabed. Fig. 7 shows the stress paths, in stress subspace (τ_{xy}/p_o vs. $(\sigma_x-\sigma_y)/2p_o$), for elements 1 to 12; they are somewhat elliptical rather than circular near the mud line. It also can be observed from Fig. 8b that the amplitudes of the effective stresses are only a little different (the shear stress τ_{xy} is less and the normal stress quantity $\sigma'_x-\sigma'_y$ is more) from the uniform elastic layer solution in spite of the remarkable difference in assumed values for Young's modulus.

NUMERICAL SOLUTION FOR EFFECTIVE STRESSES IN AN ELASTOPLASTIC SEABED

The above problem has been re-analyzed using the proposed hypoplasticity model for sand. In doing so, a set of "plastic" parameters in addition to the aforementioned elastic parameters are needed as input to the "SAC2" program. Table 2 gives the input data used in the analysis. The plasticity model parameters for the North Sea location soil are not available, those listed in Table 2 are derived from the true triaxial test results on loose Fuji River sand reported by Yamada and Ishihara (22).

An inherent difficulty in solving plasticity problems for soil structure is the historical dependence, which is not encountered in elastic solutions. The seabed is assumed initially in the "at rest" state, i.e. the wave height equals zero at t = 0 and the initial stress state is assumed as normally consolidated, i.e. $\sigma'_{xo} = \sigma'_{yo} = \sigma'_{zo} = \gamma y$.

TABLE 2. Parameters for hypoplasticity model for sand

Conventional Sand Property Parameters:
Consolidation Coefficients: $\lambda = 0.14$, $\kappa = 0.01$
Critical state line: $M_c = 1.47$, $M_e = M_c$
Phase Transformation Line: $M_{cp} = 1.24$
Elastic Shear Modulus Index: $G_e = 100$
Model Parameters: (20)
Plastic Shear Modulus Index: $H_{rp} = 0.1$
Plastic Index on Flat Cap: $Z_{et} = 1.0$
Shear Compaction Parameters: $A_c = 2.5$, $A_e = 2.5$, $B_c = 4.5$, $B_e = 4.5$

The travelling wave is then assumed to gradually increase in amplitude, this process can be simply expressed as,

$$p = p_o \, (1-\exp(-\beta t/T_o) \, \exp(i(\lambda x-\omega t)) \qquad (5)$$

Here β is a decay coefficient, controlling the amplitude of the wave loading as it approaches a desired steady state value p_o. This procedure seems unavoidable, so that in calculation a duration of several wave periods is needed in order to establish a steady state harmonic wave loading.

The stress paths during the "build-up" period are shown in Fig. 9a and b. After the first cycle (for instance the first cycle stress path for element 7 is oabc in Fig. 9a) the deviatoric stress paths in the stress subspace (τ_{xy}, $(\sigma_x-\sigma_y)/2$) approach circular paths. In Fig. 10 the stress paths of the third wave cycle are plotted, they are similar to the stress paths obtained from solutions for the elastic layered sea-

bed in Fig. 7b. Elements near the seabed surface (11 and 12) have elliptic paths that are slightly smaller than obtained by the elastic solution (Fig. 7). The amplitudes of the effective stress and pore water pressure distributions with depth for the third cycle are plotted in Figs. 11a through 11e. Due to the generation of residual pore water pressure, which is the consequence of the tendency for plastic volumetric deformation, the average pore pressure fluctuation during a wave period is not zero, as can be seen from Figure 11a. This phenomenon is clearer in the time history plots for the pore water pressure and stress components σ_x', σ_y' and σ'_z (Fig. 12b,c,d). The discrepancy with the elastic solution is a result of the elastic solution's inability to account for the generation of residual pore water pressure. The quantity σ_z' increases monotonically with time (Fig. 12b), while in the elastic solution it is zero.

Since the excess pore water pressure is "cycle number" dependent, a longer storm duration (or higher wave frequency) will produce higher excess pore water pressures. The residual pore water pressure level is controlled by the balance between the rate of pore water pressure generation and dissipation in a sand deposit which depends on wave height, wave period, and the sand permeability; in an elastic material, however, all the pore water pressure is transient and is not dependent on wave duration.

FAILURE CRITERIA

The above predicted stress distribution in the soil is the wave induced incremental change from the initial equilibrium state σ_{xo}, σ_{yo}, σ_{zo}. The global effective stress is the sum of the initial and the wave induced components, i.e.,

$$\sigma'_{xx} = \sigma'_{xo} + \sigma'_{x},\ \sigma'_{yy} = \sigma'_{yo} + \sigma'_{y},\ \sigma'_{zz} = \sigma'_{zo} + \sigma'_{z},\ \sigma'_{xy} = \sigma'_{xy} \tag{6}$$

where σ_{yo} is the initial effective vertical normal stress given as

$$\sigma'_{yo} = \gamma y \tag{7}$$

and γ is the bouyant unit weight of the soil. The quantities σ'_{xo} and σ'_{zo} may be expressed as

$$\sigma'_{xo} = \sigma'_{zo} = K_o \sigma'_{yo} \tag{8}$$

where K_o ranges from 0.4 to 1.0.

Yamamoto (23) proposed a failure criterion based on a critical 'stress angle', i.e.,

$$\sin\phi(x,y,t) = \sqrt{(\sigma'_{xx}-\sigma'_{yy})^2 + 4(\tau_{xy}^2)} \Big/ (\sigma'_{xx}+\sigma'_{yy}) \tag{9}$$

The failure state of the sandy soil at a given point and a given instance is defined as

$$|\phi(x,y,t)| \geq \phi_f \tag{10}$$

where ϕ_f is the angle of internal friction of the soil.

In a recent paper, Okusa (17) suggested the use of one of the following two simple criteria for predicting instability of seabed soil i.e.: the vertical effective stress $\sigma'_{yy} = 0$, or the mean normal pressure $\sigma'_{kk}/3 = 0$. The failure criteria cited above have been applied to the elastic solutions, a 'tensile stress' zone was predicted near the mud line (surface of the seabed), which was called the 'liquefied' zone.

Since the shear strength of sandy soil is confining pressure dependent, the reduction of shear strength due to decreasing confining pres-

sure, may cause soil to failure. In light of this, a brief discussion of Yamomodo's criterion is given below.

In the case of an elastic soil, the sum of the induced stresses $(\sigma'_{xx} + \sigma'_{yy})$ (perhaps a better index is the mean confining pressure $p = \sigma'_{kk}/3 = 1/3(\sigma'_{xx} + \sigma'_{yy} + \sigma'_{zz})$) repeats itself periodically. Thus failure due to a harmonic wave loading would be reached in the first wave cycle or not at all, i.e. it is not "history dependent". However, in the case of an elastoplastic soil, the sum of the global effective stresses $(\sigma'_{xx} + \sigma'_{yy})$ can with time be reduced due to the buildup of residual pore water pressure. This is demonstrated clearly in Fig. 13, in which the effective stress path in the σ'_{kk} vs. τ_{xy} stress subspace is shifting towards the left, thus reducing the confining pressure. As a consequence, the stress angle $|\phi(x,y,t)|$ will increase with cycle number and eventually will reach the ultimate value which is either a steady state, or a failure state. This indicates another type of failure - a progressive failure due to accumulated residual pore water pressure; and further, it implies that the stability analysis of a seabed based on an elastic analysis might overestimate its safety. Thus, seabed failure depends not only on the magnitude of a storm, but also on its duration, i.e. how long it lasts.

To this point the significant difference of failure analyses which are based on the same failure criterion but use either elastic (or visco-elastic) and plastic soil model have been discussed. An in-depth study of the pore pressure failure phenomenon using the proposed approach would perhaps be more meaningful and should be a topic of further investigation.

COMPARISONS WITH WAVE TANK EXPERIMENT

A wave tank experiment conducted at Cornell University was reported by Clucky, et al. (3). The tests were carried out in a 17.1m wave facility, in which the central portion contained a 4.57m long sediment bay allowing a B = 0.84m deep deposit to be placed. The relevent hydrodynamic properties included the unit weight of water (9.8 kN/m^3), water depth D (0.53m), wave period T (from 1.32s to 2.49s), and wave length L (which was determined from the wave period T and the water depth D using linearized or small amplitude wave theory).

Several sand parameters were also provided, i.e., shear modulus G(640 kN/m^2), Poisson's ratio (0.33), permeability k (1.1×10^{-3} m/s), porosity n(42%), void ratio e (0.720), and dry unit weight (15.36 kN/m^3). The bulk modulus of water $2.0 \times 10^9 N/m^2$ was used in the calculations. Other parameters needed in the plasticity model were assumed, as previously discussed, from the Fuji River sand result (see Table 2).

In performing the analysis, the F.E. mesh extends in the horizontal direction one complete wave length. In the following example for a wave period T = 1.32s the calculated wave length is 2.4m, which is 3 times the depth of the sand deposit (B = 0.84m). The boundary conditions at the tank bottom were assumed to yield neither displacement nor flow, i.e.

$$u = 0,\ v = 0,\ \text{and}\ dp/dy = 0 \quad ,\ \text{at}\ y = -B \tag{11}$$

The sand deposit for the analysis is divided into 144 elements and the nodes are equally spaced in both the vertical and horizontal directions. The stresses plotted in the following figures are wave induced stresses over and above the initial normally consolidated states.

It is well known that plasticity solutions yield a nonlinear response with loading amplitude, so that the normalized stress quantities σ'_x/p_o, σ'_y/p_o, σ_{xy}/p_o change with wave amplitude p_o. The only available information related to p_o is the wave height which is given in the Abstract of reference (3) as "up to 0.28m". Based on the linear wave theory, an estimated value of $p_o = 0.6$ kN/m^2 is adopted for this analysis.

First, an elastic analysis was performed using the "SAC2" program. Fig. 14 shows the predicted stress paths for the water tank experiment based on the elastic solution. Since the tank is relatively shallow in comparison with the wave length, the sand at different depths experiences elliptic loading paths in the τ_{xy}/p_o via $(\sigma_x-\sigma_y)/2p_o$ stress subspace. The shear stress τ_{xy} near the surface (element 12, Fig. 14b) is very small thus the elliptical stress path has its long axis in the $(\sigma_x-\sigma_y)/2p_o$ direction. However, due to friction between the sand and the tank bottom, the bottom layer (element 1) experiences a large shear stress and its deviatoric stress component is reduced thus the long axis of the stress path lies in the shear stress direction. Stress paths in between the upper and lower elements are less influenced by the boundary conditions.

The amplitudes of the stresses during the third loading cycle from the elastic solution are plotted in Figs. 15a to 15e; they are symmetrical about the vertical axes. Also one can see from Fig. 16 that the time history of the stresses tends to reach a harmonic state after the third cycle.

The plasticity solution was also obtained using the "SAC2" program which included the model code "SAND" developed by the authors. The stress paths are shown in Fig. 17 for the first two cycles. In compari-

son with the elastic solution (Fig. 14), the stress paths near the surface (elements 11 and 12) have smaller normal stress differences, due to the plasticity of the soil. This may be observed more clearly from Figure 18b, where the predicted amplitudes of the effective stress σ_y from the elastic and plastic solutions are plotted together with the experiment results. It seems clear that the plasticity solution is in better agreement with the test results.

It is worth mentioning that the residual pore water pressure is insignificant in this case due to the high permeability used in calculation ($k = 1.1 \times 10^{-2}$ m/s), more or less like a drained condition. But there is a remarkable difference in the amplitude distribution for σ'_x (Fig. 18d) after only two loading cycles. The only apparent reason for this behavior is the plastic volumetric deformation, which induced the asymmetric distribution of amplitudes and the time histories of stresses σ'_x, σ'_z in Figs. 18d,18e,19a and 19b.

The buildup of excess pore water pressure depends upon the balance between pore water pressure generation due to the plastic soil properties and dissipation due to soil permeability. Three different soil permeabilities were assumed for the wave tank experiment ($k = 0$, 1×10^{-4}, 1×10^{-2} m/s); the corresponding time history traces of the induced residual pore water pressure are shown in Fig. 19. The upward shift of the pore pressure traces for lower permeabilities is obvious. However, no shift is observed in the time history of the shear stress τ_{xy} (Fig. 19e) because the shear stress is not influenced by the rise of pore water pressure. In general, the plasticity solution for the deviatoric stress path is not symmetrical with respect to the initial stress state (i.e. $\sigma'_{xo} = \sigma'_{yo} = \sigma'_{zo}$) as shown in Fig. 17; however, if the permeability of the soil is very low (equivalent to an undrained

state), the deviatoric stress path as shown in Fig. 20 is practically symmetrical about the initial stress state; this behavior is similar to that of the elastic solution.

CONCLUSIONS

Owing to the importance of seabed stability under wave loading to off-shore engineering installations, extensive studies both theoretical and experimental have been reported. A new analytical approach using an elastoplastic constitutive model for sand is presented in this paper. Tentative conclusions may be stated as follows.

A. The amplitudes of the wave induced deviatoric stress $(\sigma_x-\sigma_y)/2$ are slightly smaller than the corresponding values for a multilayered elastic solution for layers near the seabed surface due to soil plasticity.

B. Excess pore water pressure can be generated by the rotational shear stress path. If it is not dissipated, it will be accumulated and will build up a residual pore water pressure in the seabed soil.

C. It has been demonstrated analytically that the stress paths in the deviatoric stress subspace are elliptical under harmonic wave loading for both elastic and elastoplastic soil deposits of finite depth.

D. The failure criterion based on a critical "stress angle" is suitable for seabed instability analyses. Because, in rotational shear, the deviatoric stress amplitude does not decrease to zero before it reaches failure. The "stress angle" may increase due to the increase in residual pore water pressure and may lead to failure. This "time dependent" ultimate state and/or failure cannot be predicted by elastic or viscoelastic soil models.

E. A comparison between the present solution and the wave tank experiment conducted at Cornell University seems to demonstrate that the plasticity analysis can better predict test results than the elastic analysis.

ACKNOWLEDGEMENT

The present study is partially supported by a sea grant (No. R/OT-13) under the California Sea Grant College Program. The authors are grateful for the support to initiate this study.

REFERENCES

1. Bea, R.G., Wright, S.G., Sircar, P., and Niedoroda, W., "Wave-Induced Slides in South Pass Block 70, Mississippi Delta," Journal of the Geotechnical Engineering Division, ASCE, Vol. 109, GT4, April, 1983, pp. 619-644.

2. Biot, M.A. "General Theory of Three-Dimensional Consolidation," Journal of Applied Physics, Vol. 12, 1941, pp. 155-164.

3. Clukey, E.C., Kulhawy, F.H., Liu, P.L.F., and Turcotte, B.R., "Experimental Study of Effective Stress Response of Sand Under Water Wave Loading," Offshore Technology Conference, 1984, pp. 413-418.

4. Dafalias, Y.F. and Herrmann, L.R., "Bounding Surface Formulation of Soil Plasticity," Soil Mechanics-Transient and Cyclic Loads, 1982, pp. 253-282.

5. Dafalias, Y.F., "Bounding Surface Plasticity. I: Mathematical Foundation and Hypoplasticity," Journal of Engineering Mechanics, ASCE, Vol. 112, No. 9, September, 1986, pp. 966-987.

6. Dalrymple, R.A. and Liu, P.L.F., "Wave Over Soft Muds: A Two-Layer Fluid Model," Journal of Physical Oceanography, Vol. 8, 1978, pp. 1121-1131.

7. Desai, C.S. and Siriwardane, H.J., "A Concept of Correction Functions to Account for Non-associative Characteristics of Geologic Media," International Journal for Numerical and Analytical Methods in Geomechanics, Vol. 4, No. 1, 1980, pp. 377-388.

8. Figueroa, L., Yamamoto, T., and Nagai, T., "Inverted Shear Modulus from Wave-Induced Soil Motion," Journal of Geotechnical Engineering, ASCE, Vol. III, No. 1, 1985, pp. 115-132.

9. Finn, W.D.L., Siddharthan, R., and Martin, G.R., "Response of Seafloor to Ocean Waves," Jour. of Geotechnical Engineering, ASCE, Vol. 109, No. 4, April, 1983, pp. 556-572.

10. Gade, H.G., "Effects of a Non-Rigid, Impermeable Bottom on Plane Surface Waves in Shallow Water," Journal of Marine Research, Vol. 16, 1957, pp. 61-82.

11. Herrmann, L.R. and Mish, K.D., "User's Manual for SAC-2, a Two-Dimensional Nonlinear, Time Dependent Soil Analysis Code Using the Bounding Surface Plasticity Model," Order No. N02583-83-T062, U.C. Davis.

12. Herrmann, L.R. and Mish, K.D., "Finite Element Analysis for Cohesive Soil, Stress and Consolidation Problems Using Bounding Surface Plasticity Theory," Order No. N62583-83-M-T062, U.C. Davis.

13. Herrmann, L.R., Kaliakin, V., Shen, C.K., Mish, K.D., Zhu, Z.Y., "Numerical Implementation of a Plasticity Model for Cohesive Soils," accepted by Journal of Engineering Mechanics, ASCE.

14. Hsiao, S.V. and Shemdin, O.H., "Interaction of Ocean Waves with a Soft Bottom," Journal of Physical Oceanography, Vol. 10, 1980, pp. 605-610.

15. Ishihara, K. and Towhara, I., "Sand Response to Cyclic Rotation of Principal Stress Directions as Induced by Wave Loads," Soils and Foundations, Vol. 23, No. 4, 1983, pp. 12-26.

16. Madsen, O.S., "Wave-Induced Pore Pressures and Effective Stresses in a Porous Bed," Geotechnique, Vol. 28, 1978, pp. 377-393.

17. Okusa, S., "Wave-Induced Stresses in Unsaturated Submarine Sediments," Geotechnique 35, No. 4, 1985, pp. 517-532.

18. Putnam, J.A., "Loss of Wave Energy Due to Percolation in a Permeable Sea Bottom," Transactions, American Geophysical Union, Vol. 30, 1949, pp. 349-356.

19. Seed, H.B. adn Rahman, M.S., "Analysis for Wave-Induced Liquefaction in Relation to Ocean Floor Stability," Report No. UCB/TE-27/02, University of California, Berkeley, Calif., May, 1977.

20. Wang, Z.L., Shen, C.K., Dafalias, Y.F., Yang, H.W. and Li, X.S., "The Role of Relative Density in a Bounding Surface Plasticity Model for Sand," Proceedings of the 2nd Int. Conf. on Soil Dynamics and Earthquake Engineering, 1985, pp. 2-77 - 2-92.

21. Wang, Z.L., Dafalias, Y.F., and Shen, C.K., "A Hypoplasticity Soil Model for Sand," In Preparation.

22. Yamada, Y., and Ishihara, K., "Undrained Deformation Characteristics of Sand in Multi-Directional Shear," Soils and Foundations, Vol. 23, No. 1, March, 1983, pp. 61-79.

23. Yamamoto, T., "Sea Bed Instability From Waves," Offshore Technology Conference, Paper OTC 3262, 1978, pp. 1819-1828.

24. Yamamoto, T., "Wave-Induced Pore Pressures and Effective Stresses in Inhomogeneous Seabed Foundations," Ocean Engineering, Vol. 8, 1981, pp. 1-16.

25. Yamamoto, T., "On the Response of a Coulomb-Damped Poroelastic Bed to Water Waves," Marine Geotechnology, Vol. 5, No. 2, 1983, pp. 93-130.

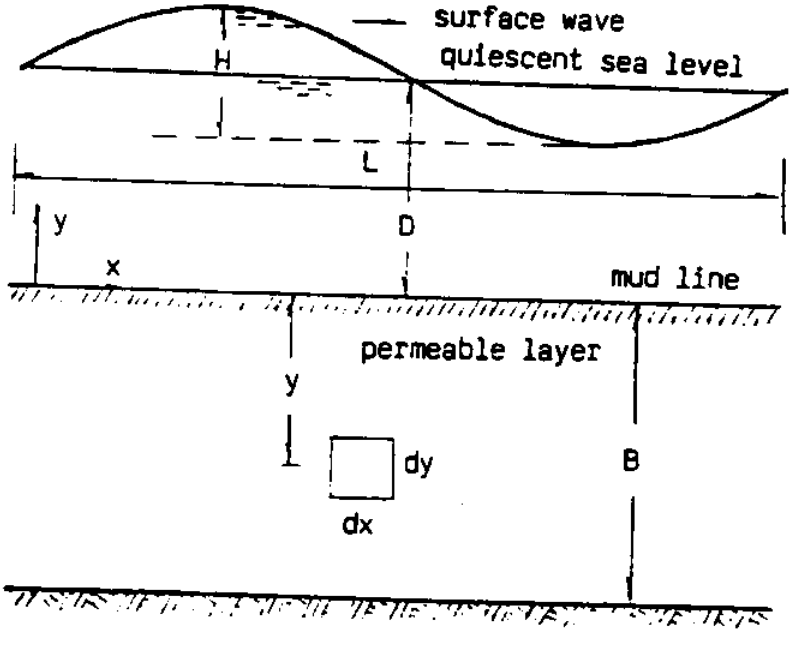

Fig. 1. Seabed under wave loading

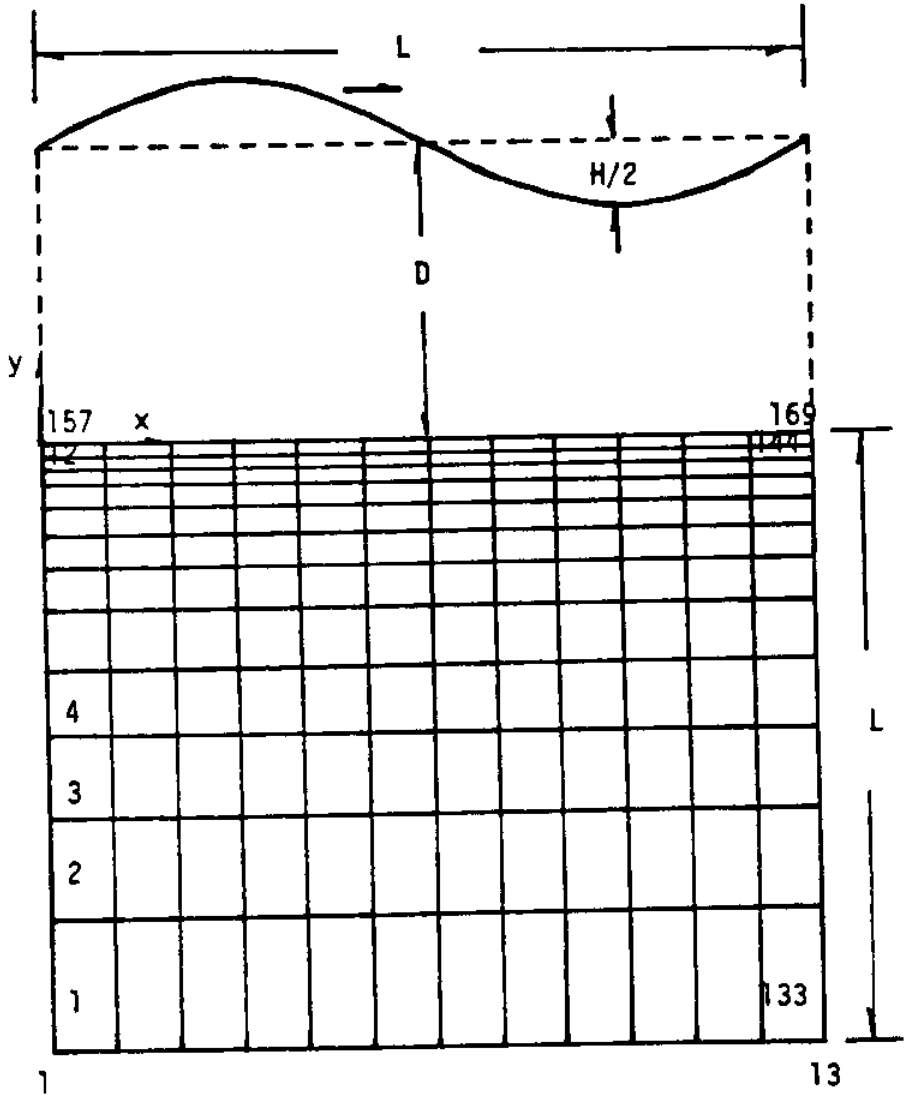

Fig. 2. Finite element mesh and wave loading

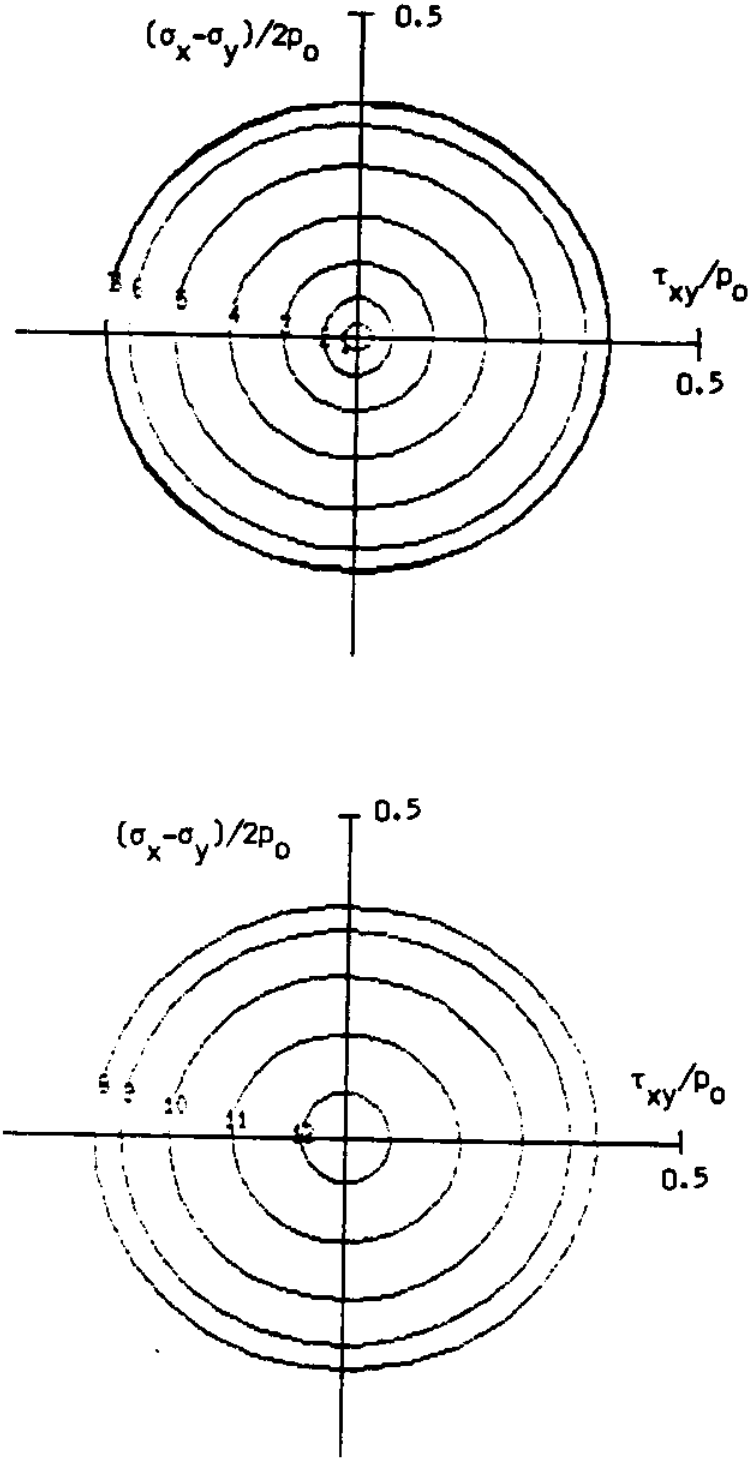

Fig. 3. Stress paths of seabed layers, elastic solution (from bottom to mudline numbering 1 to 12)

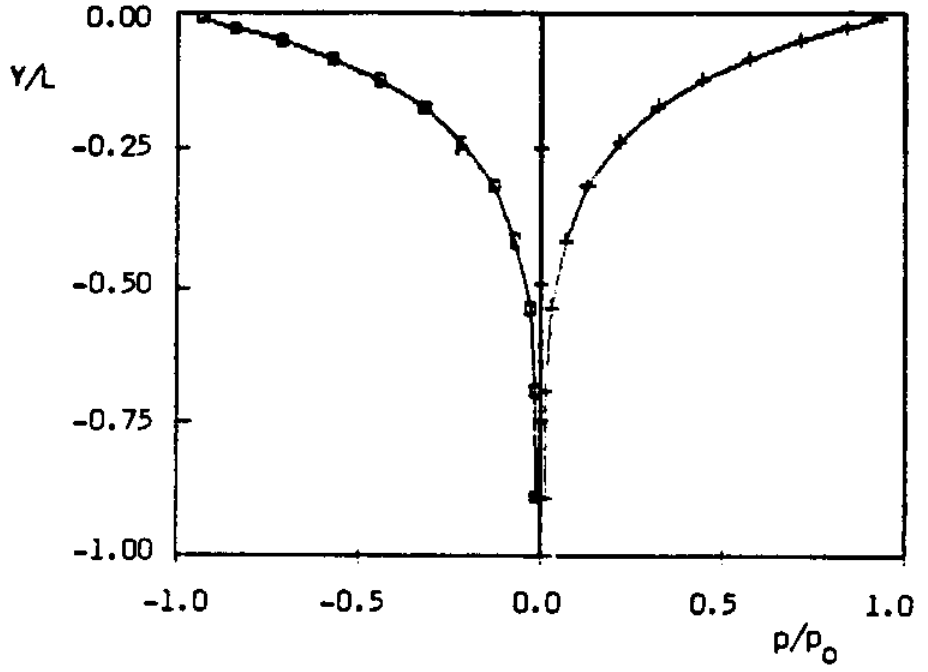

a) pore water pressure p vs depth y

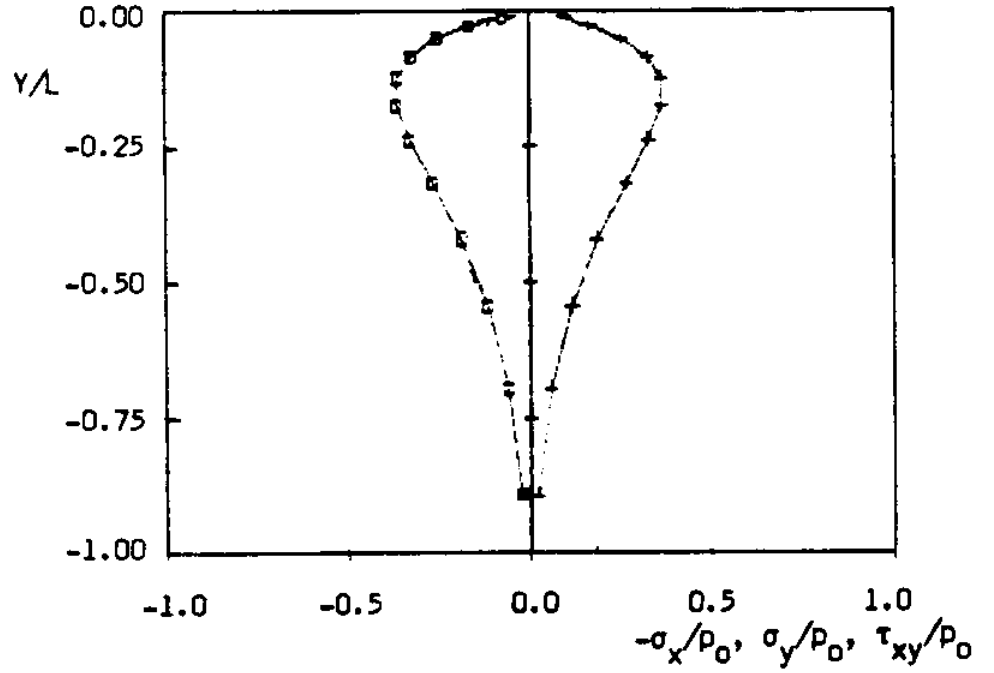

b) stresses σ_x, σ_y, τ_{xy} vs. depth y

Fig. 4. Amplitudes of stresses vs depth (elastic solution)

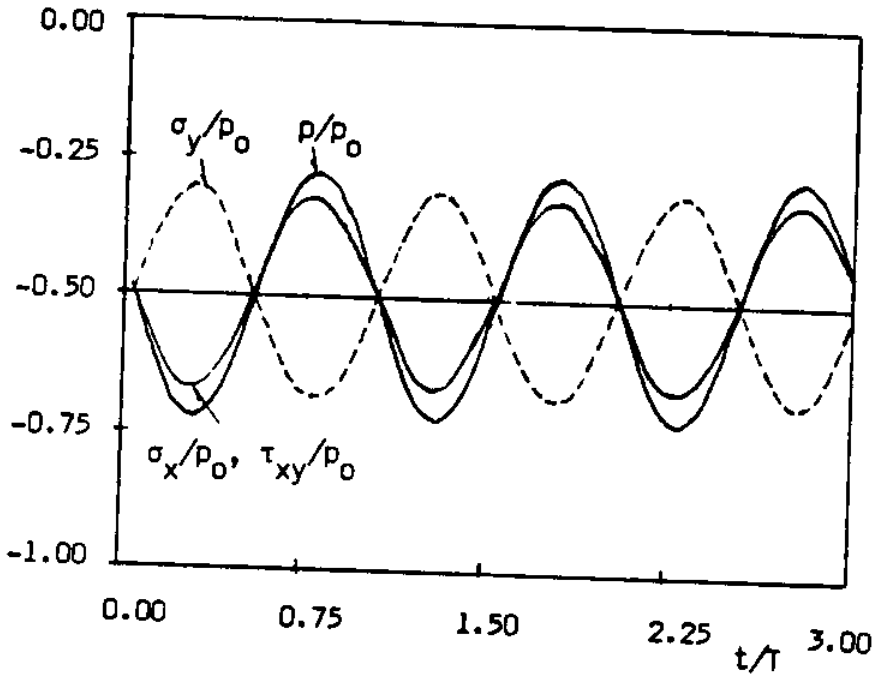

Fig. 5. Time history of p, σ_x, σ_y, τ_{xy} in element 8 (elastic solution)

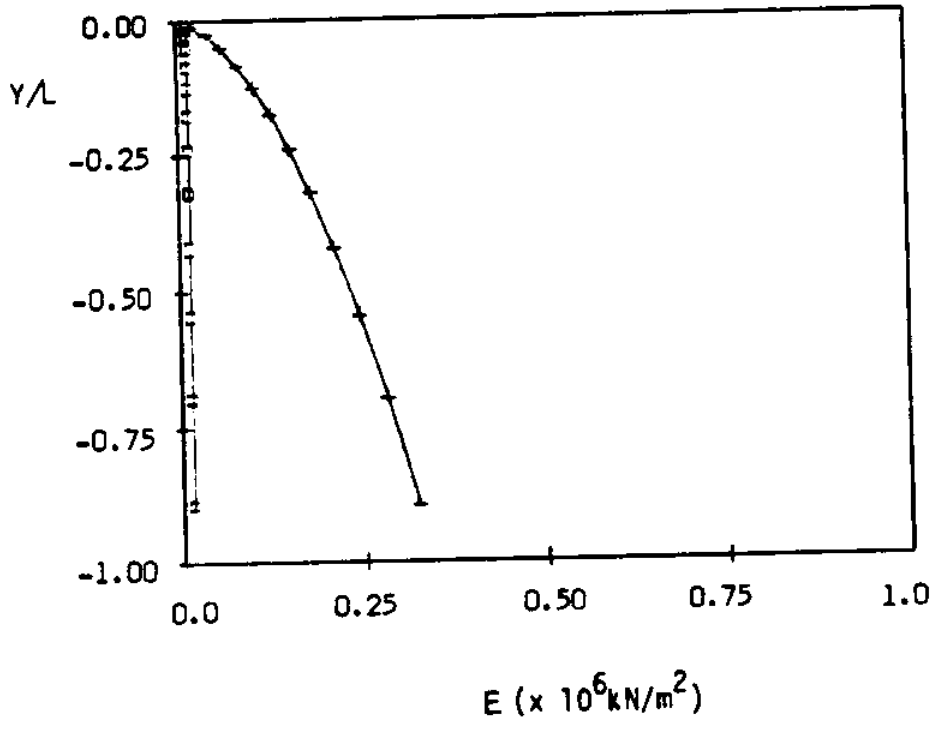

Fig. 6. Young's modulus variation along depth
for multilayered elastic solution

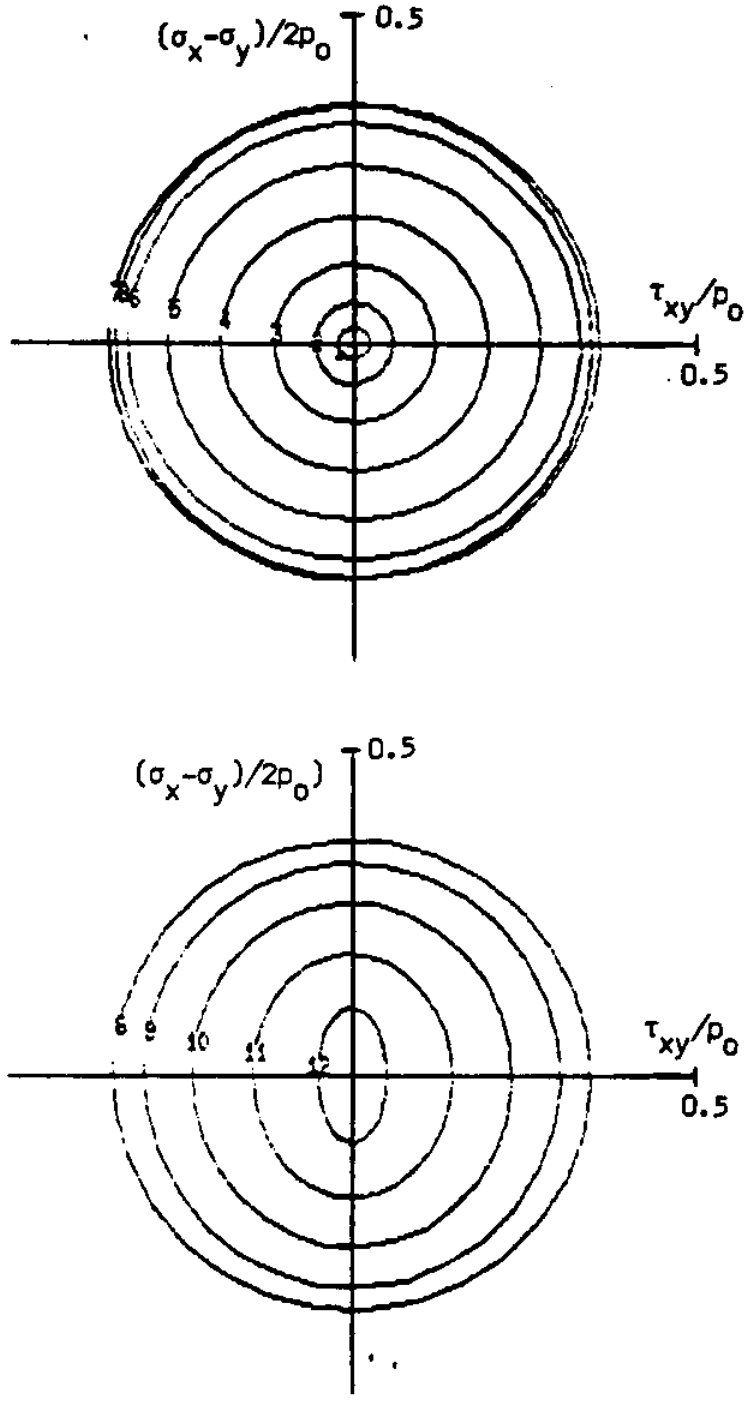

Fig. 7. Stress paths of seabed elements 1 to 12 (multilayered elastic solution)

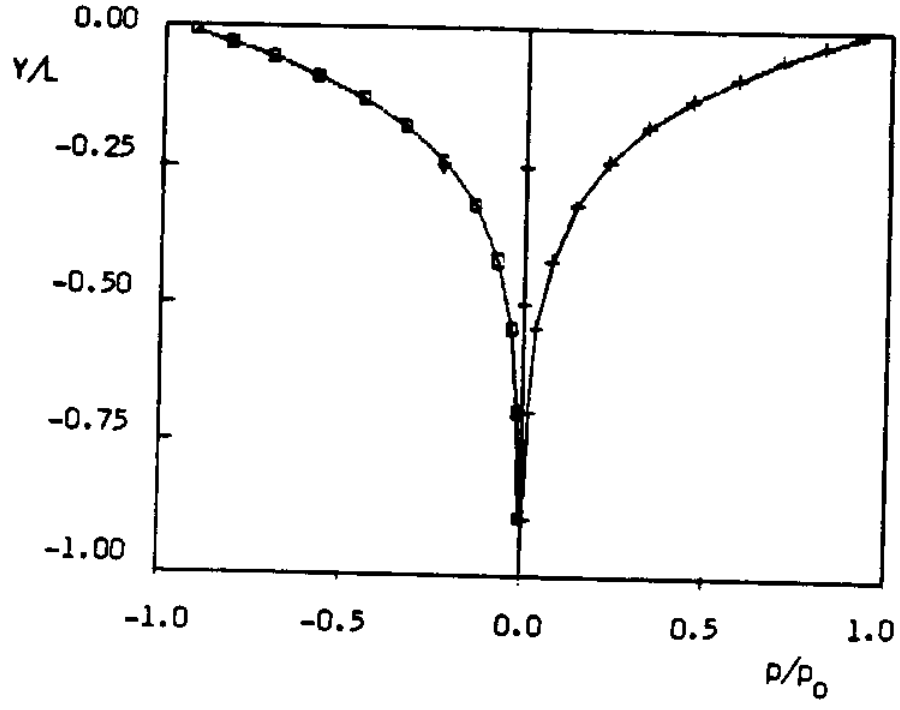

a) pore water pressure p vs depth y

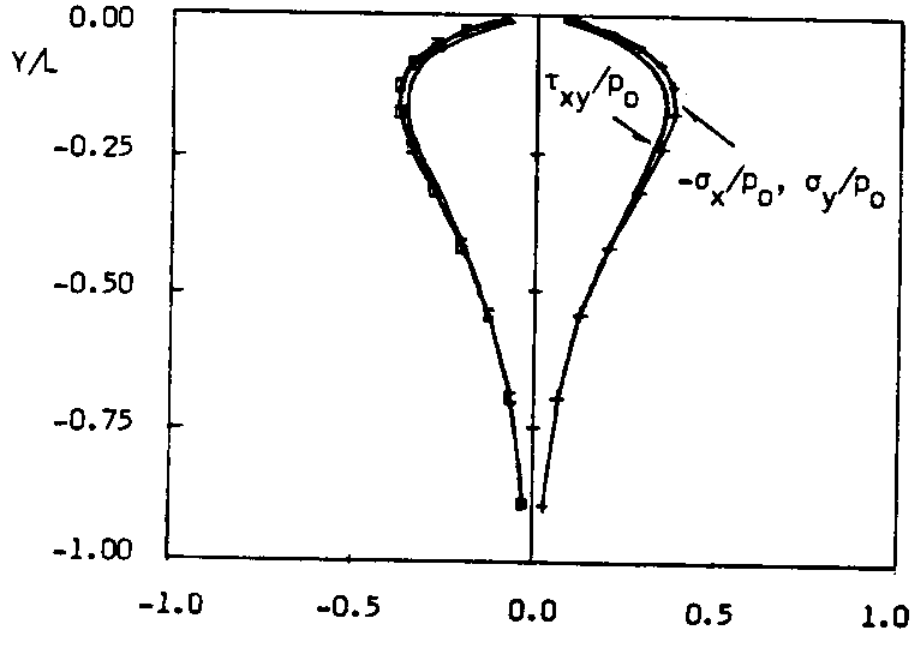

b) stresses σ_x, σ_y, τ_{xy} vs depth y

Fig. 8. Amplitudes of stresses vs depth (multilayered elastic solution)

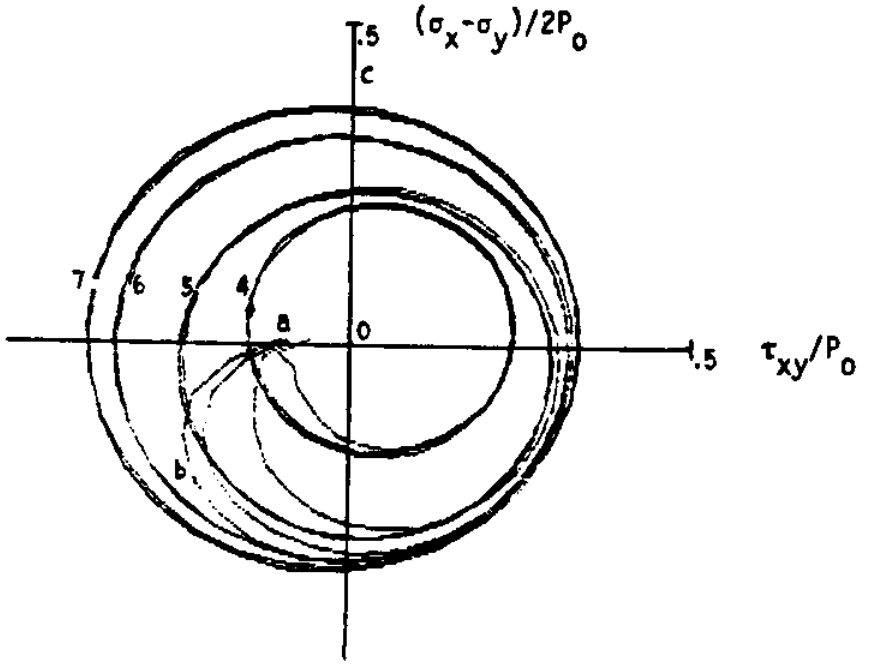

a) elements 4 to 7

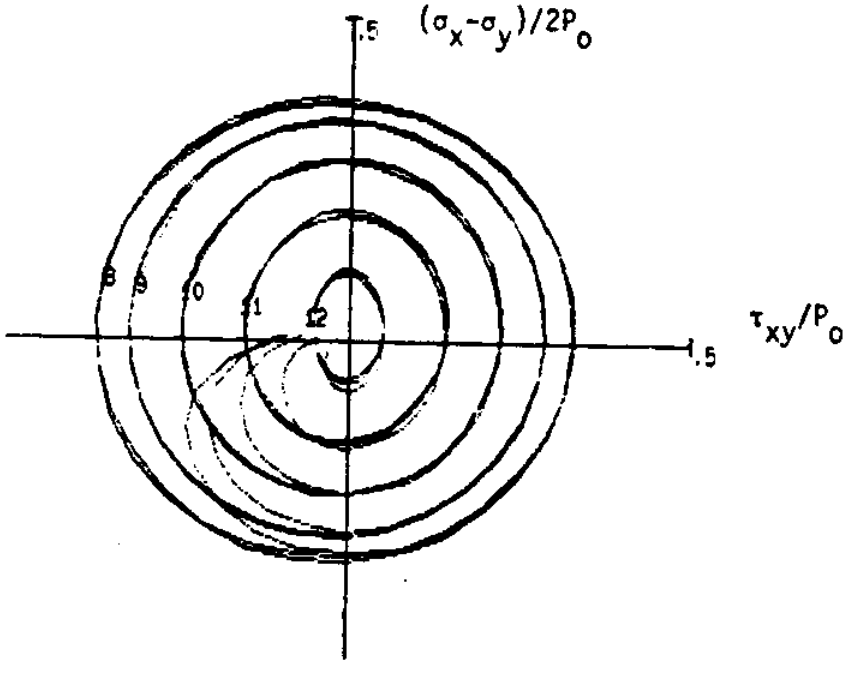

b) elements 8 to 12

Fig. 9. Stress paths in a seabed (elastoplastic solution)

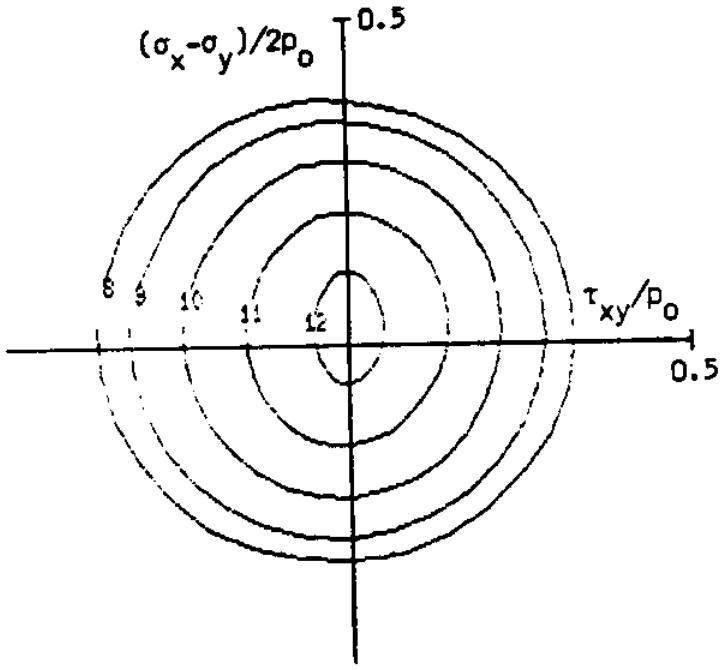

Fig. 10. Stress paths of elements 8 to 12 during the third loading cycle (elastoplastic solution)

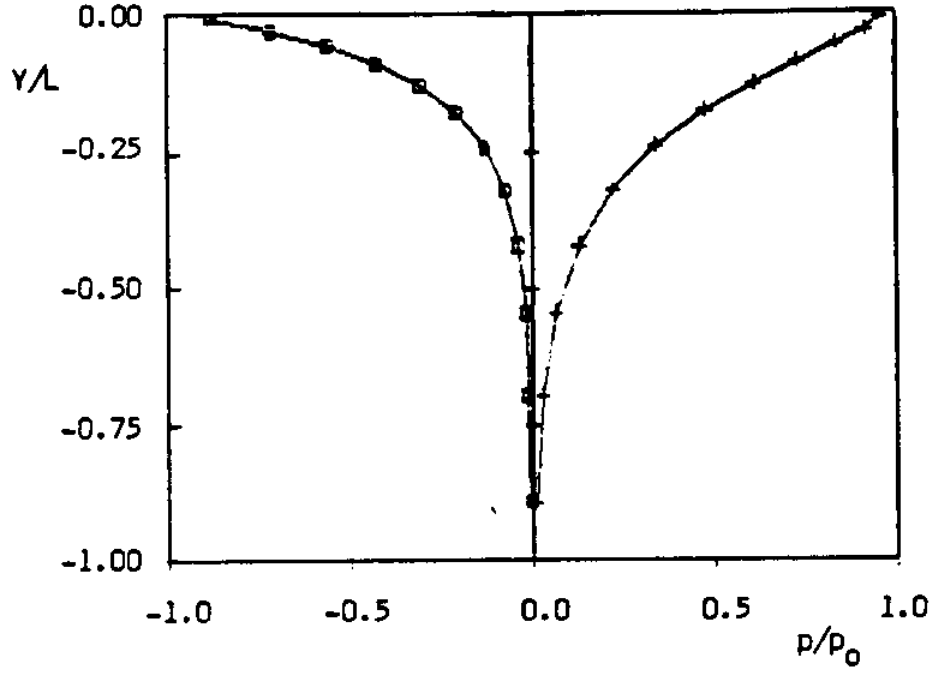

a) Pore water pressure p

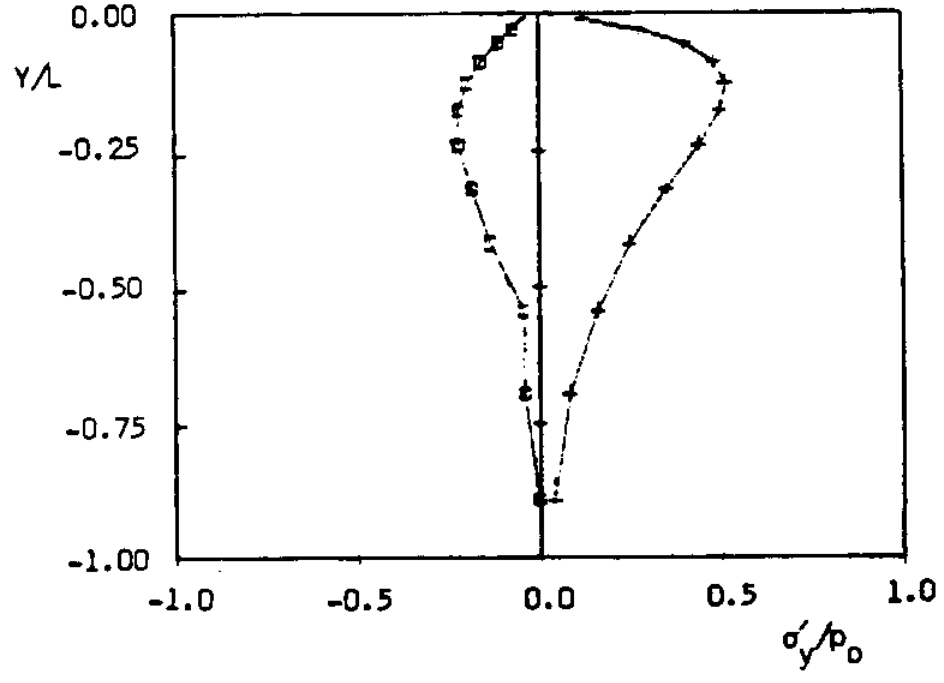

b) Effective stress σ'_y

Fig. 11. Amplitudes of stresses during the third loading cycle (elastoplastic solution)

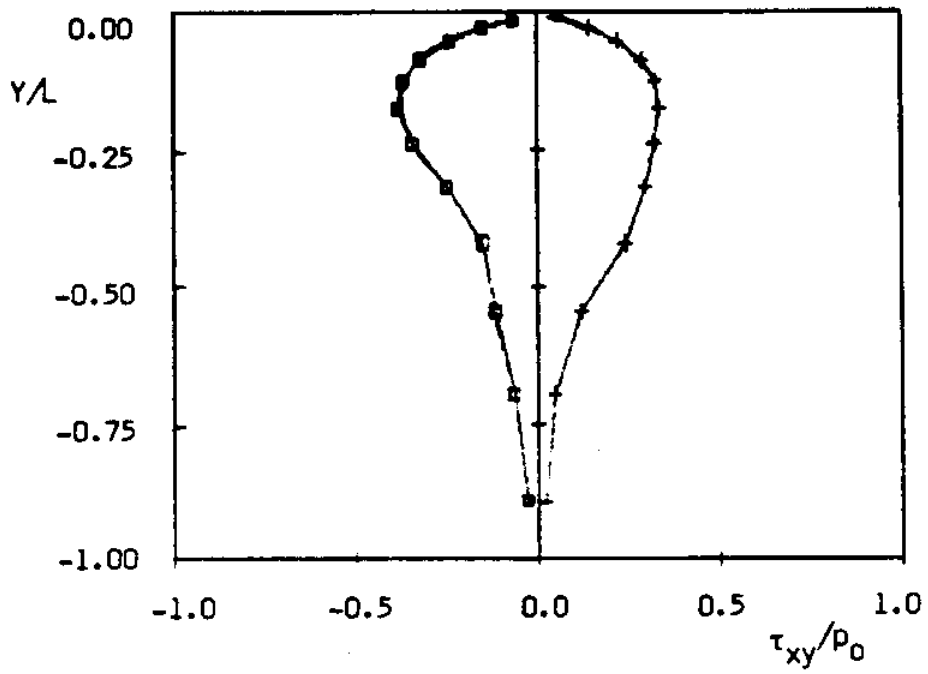

11.c) effective stress τ_{xy}

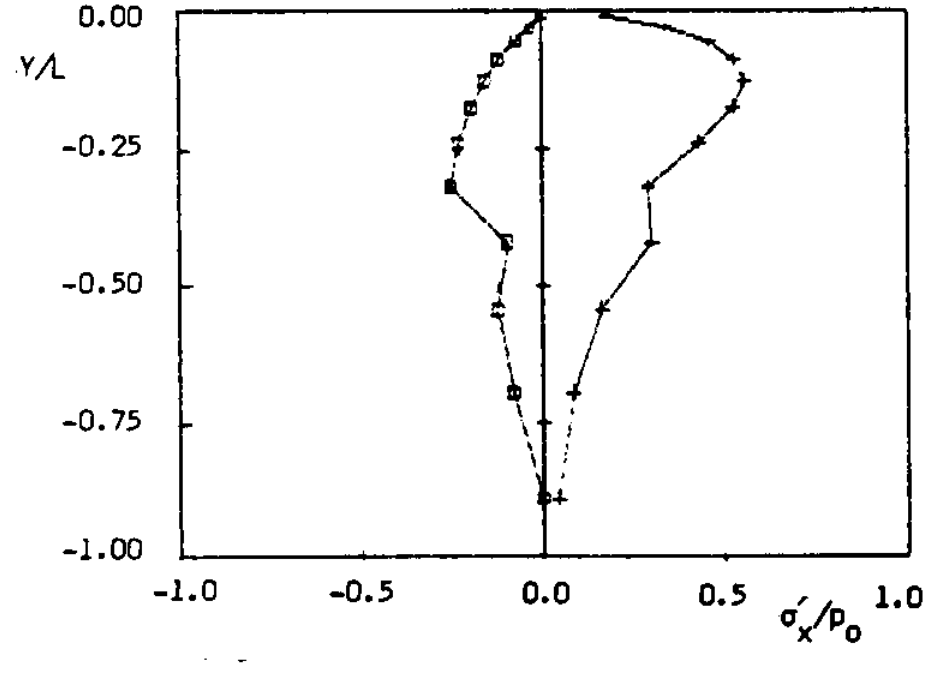

11.d) effective stress σ'_x

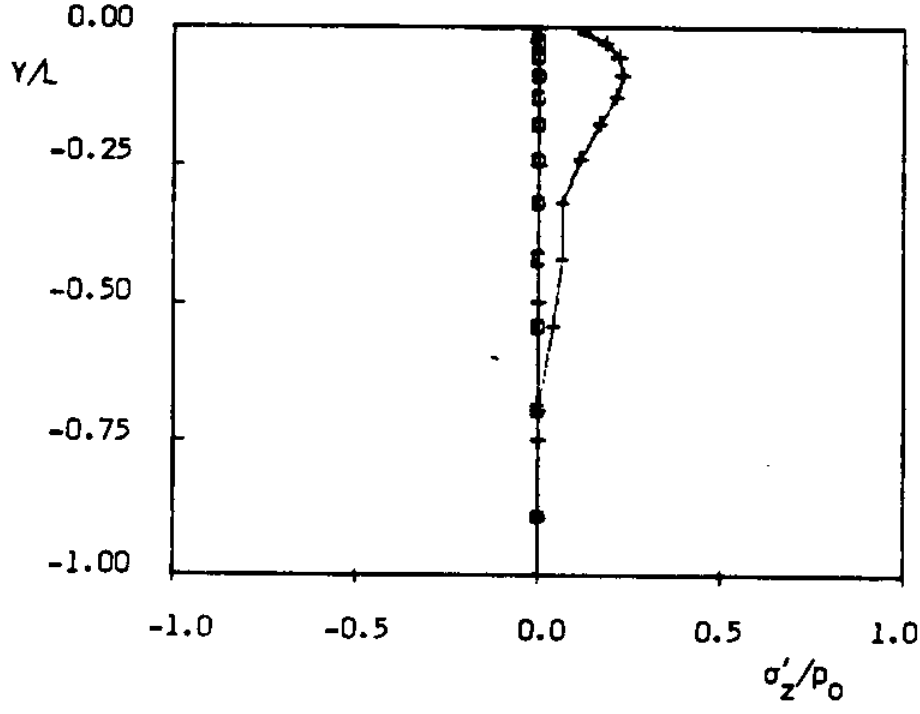

11.e) effective stress σ'_z

▫-▫- elastic solution

+-+-+ elastoplastic solution

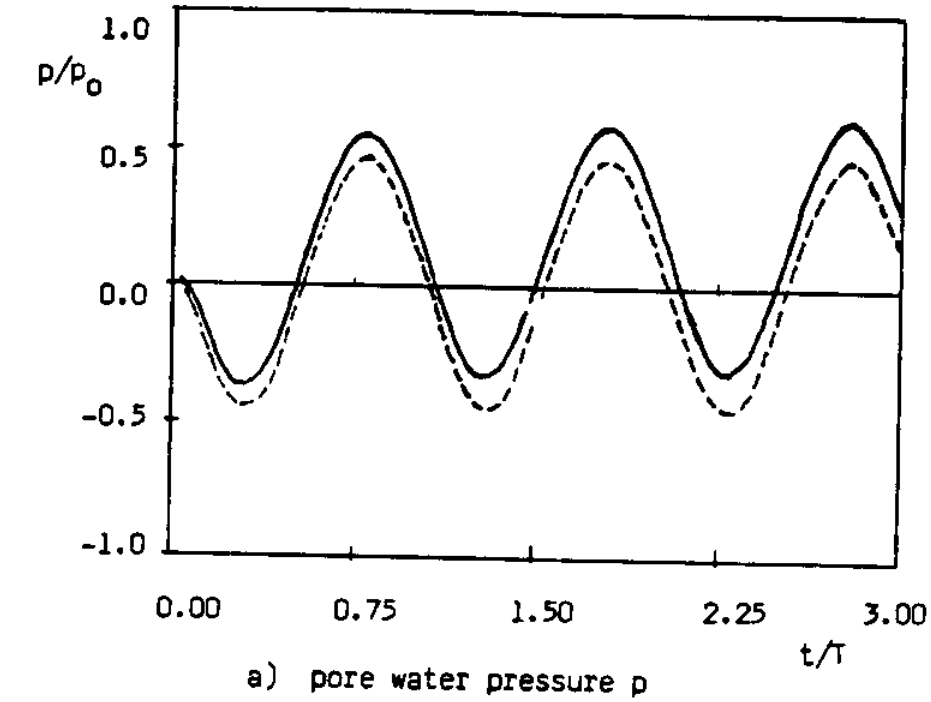

a) pore water pressure p

——— elastoplastic solution

----- elastic solution

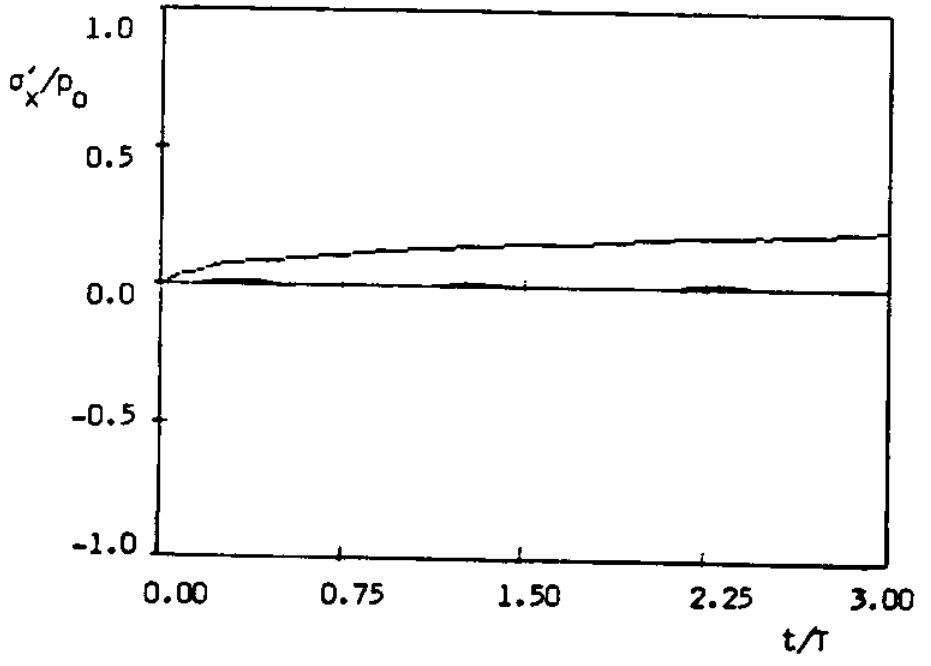

b) lateral effective stress σ'_z

Fig. 12. Time history of stresses in element 8 (elastoplastic solution)

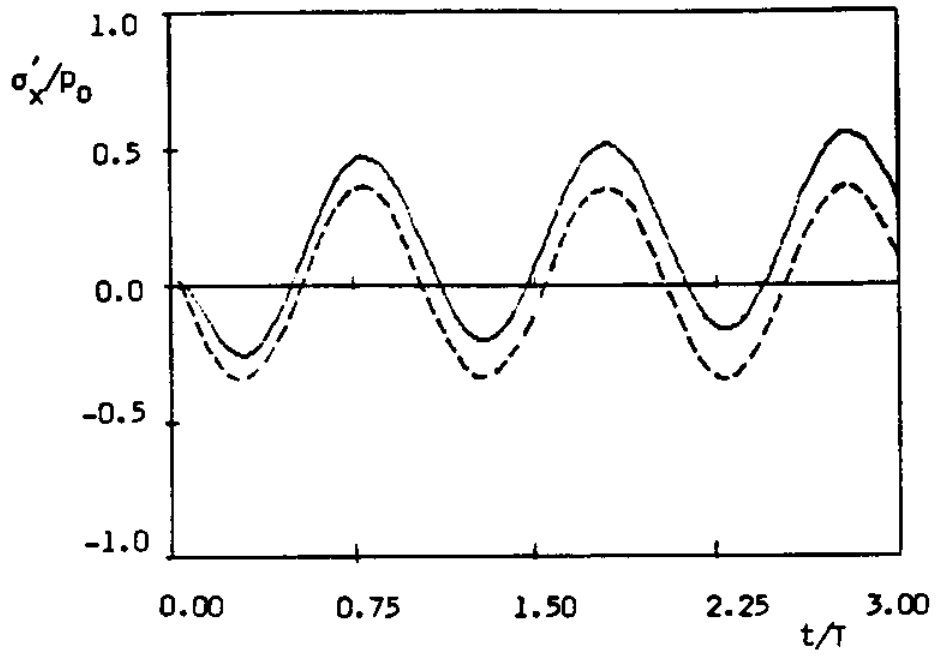

12.c) horizontal effective stress σ'_x

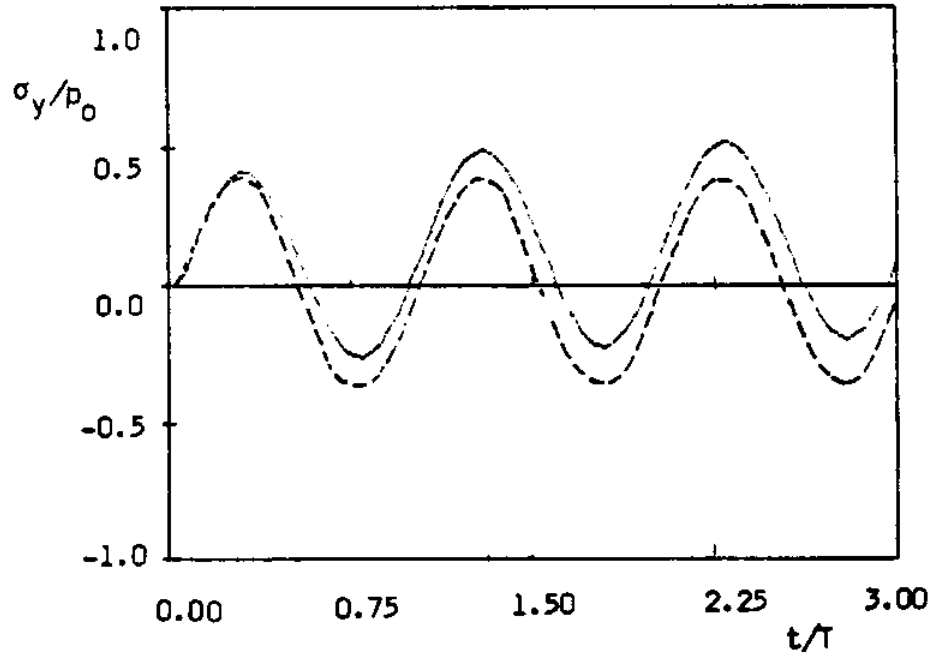

12.d) vertical effective stress σ_y

----- elastic solution

——— elastoplastic solution

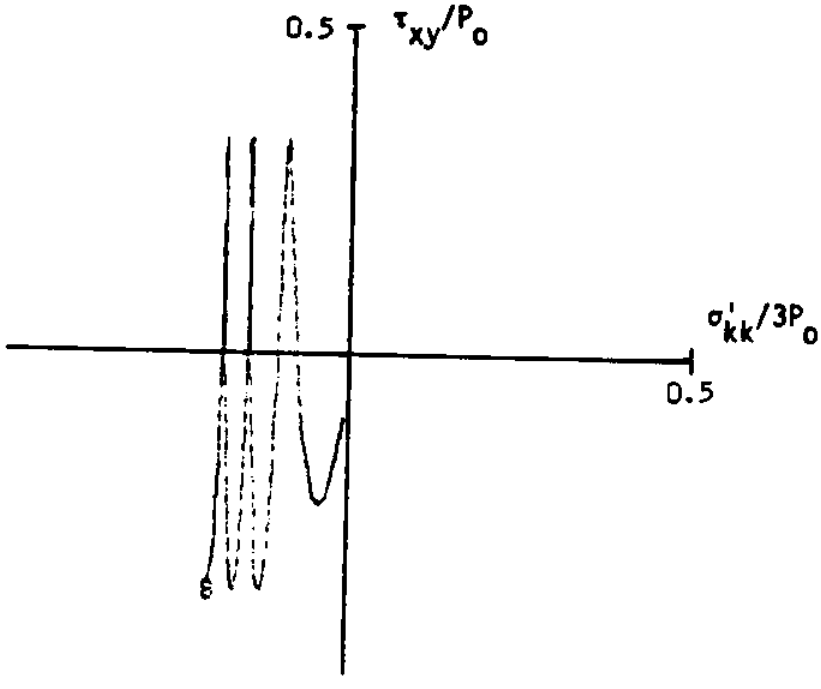

Fig. 13. Effective stress path τ_{xy} vs $\sigma'_{kk}/3$ in element 8 (elastoplastic solution)

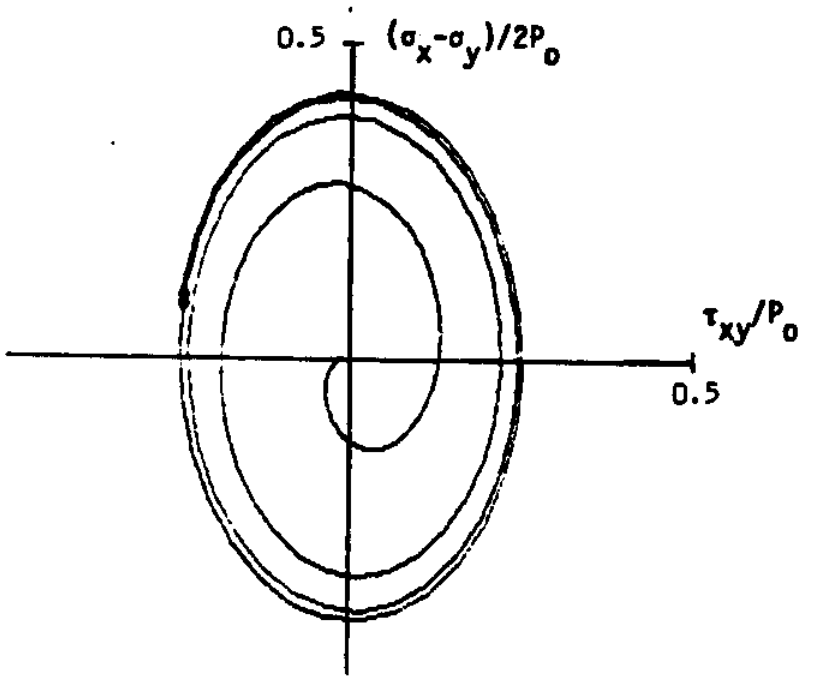

a) stress path of element 8

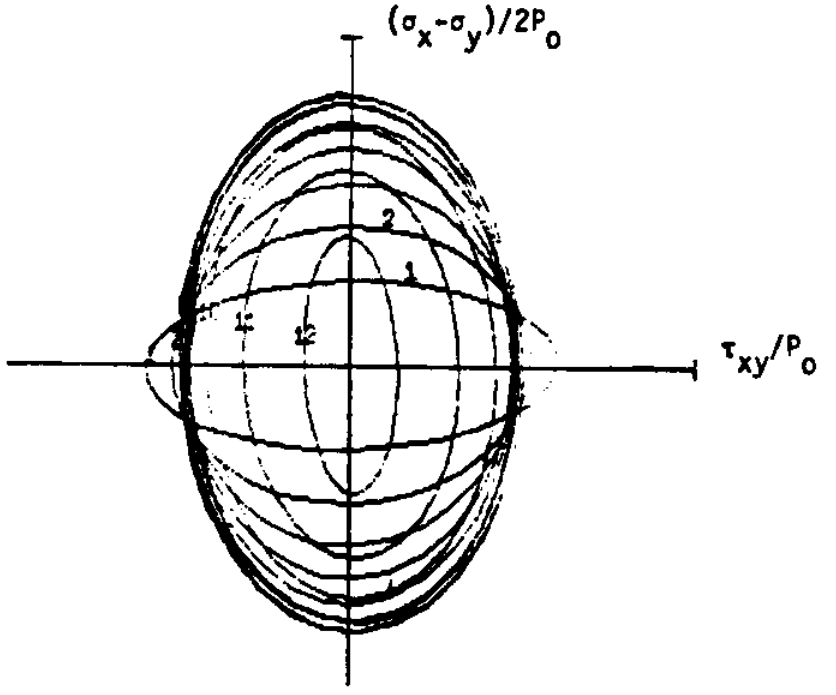

b) stress paths during the third loading cycle

Fig. 14. Stress paths of the wave tank deposit (elastic solution)

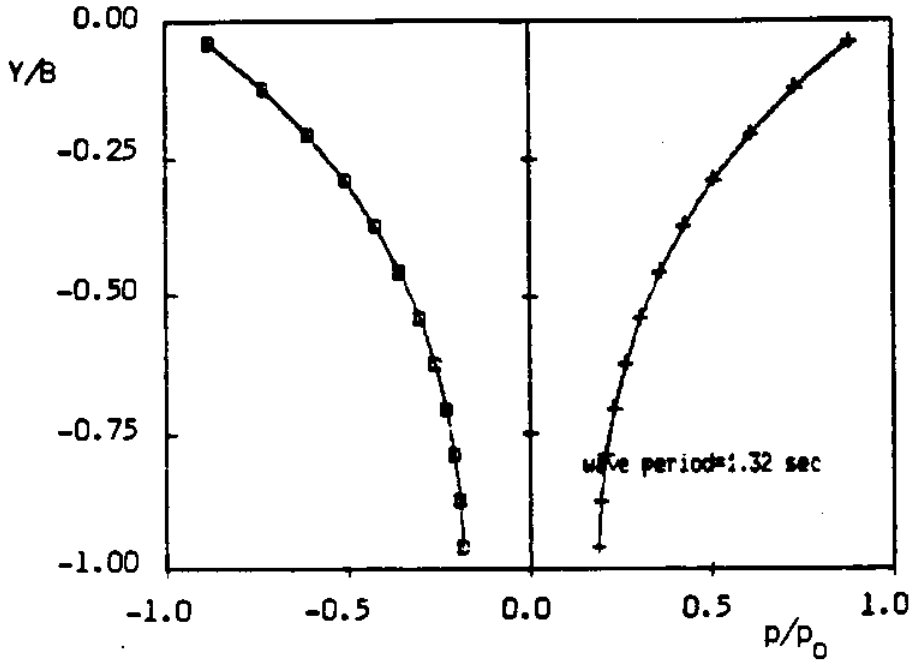

a) pore water pressure p

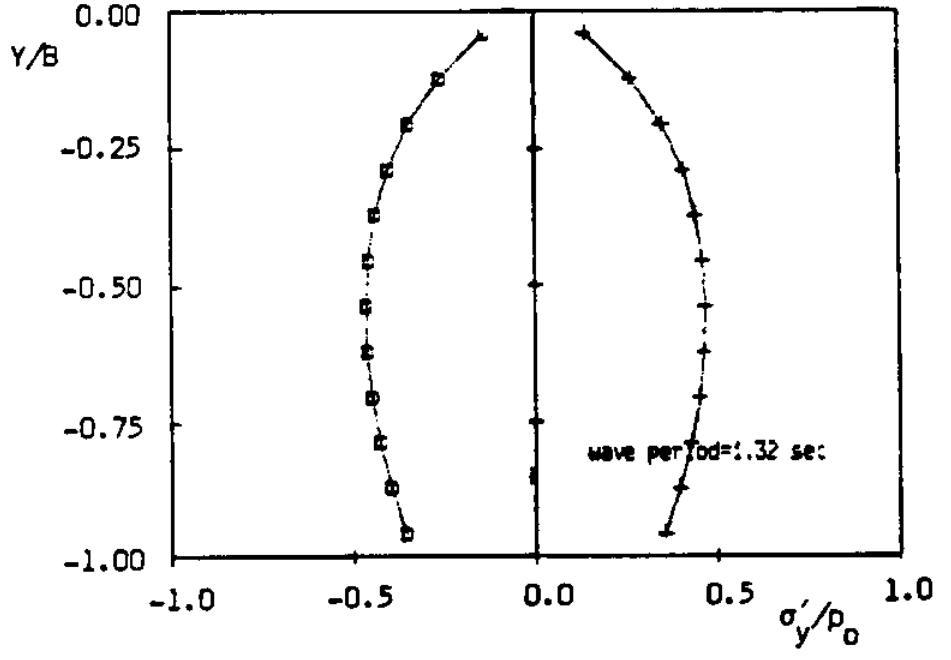

b) vertical effective stress σ'_y

Fig. 15. Amplitudes of stresses in the wave tank deposit (elastic solution)

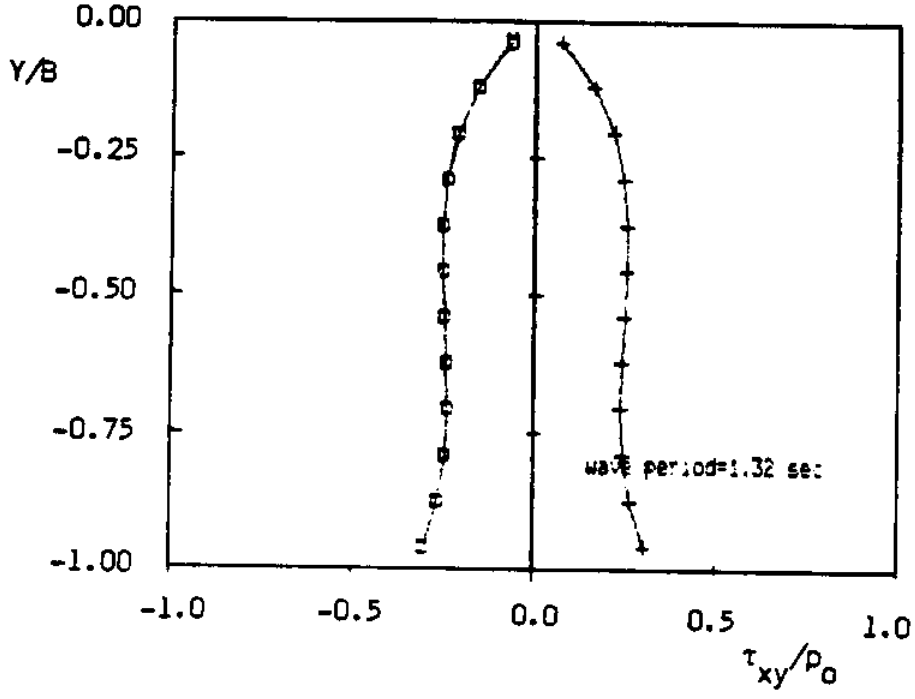

15.c) shear stress τ_{xy}

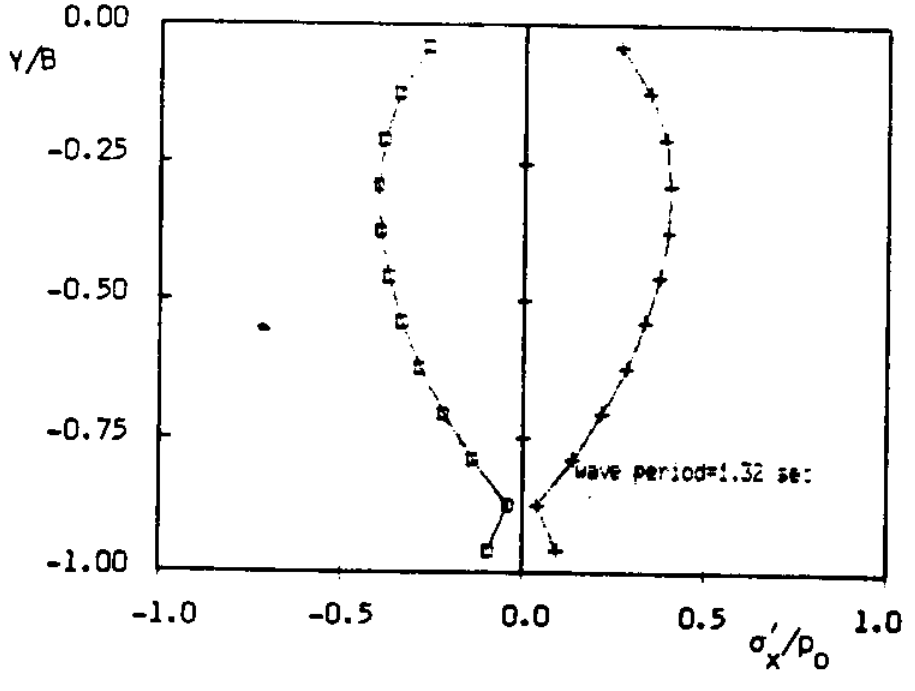

15.d) horizonal effective stress σ'_x

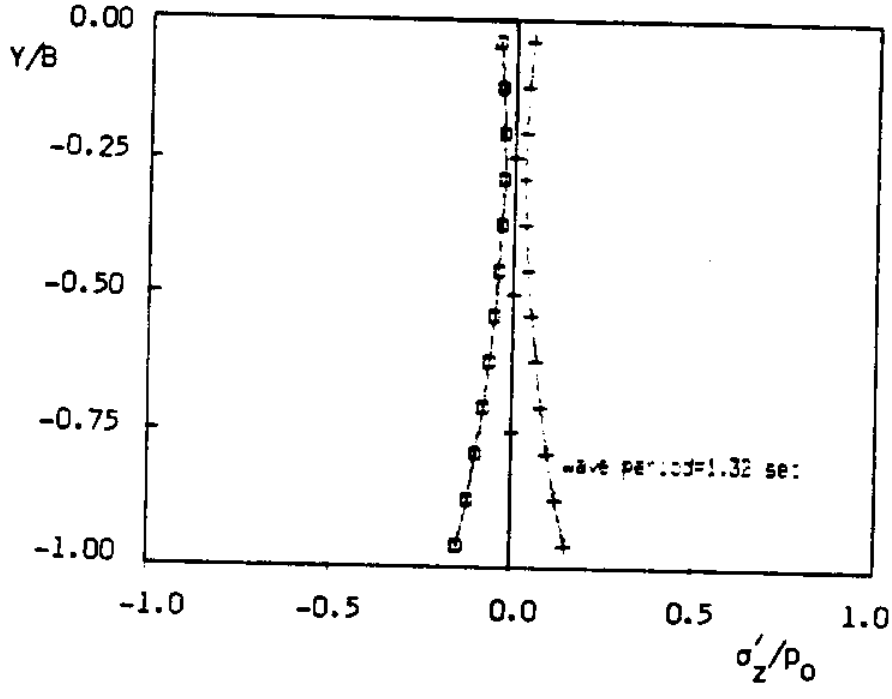

15.e) lateral effective stress σ'_z

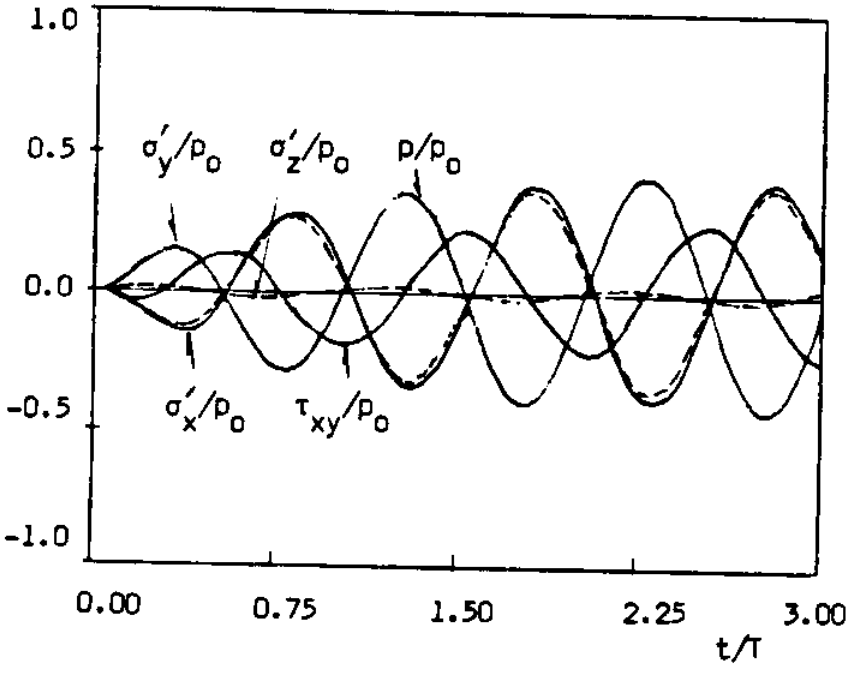

Fig. 16. Time history of element 8 in the wave tank deposit

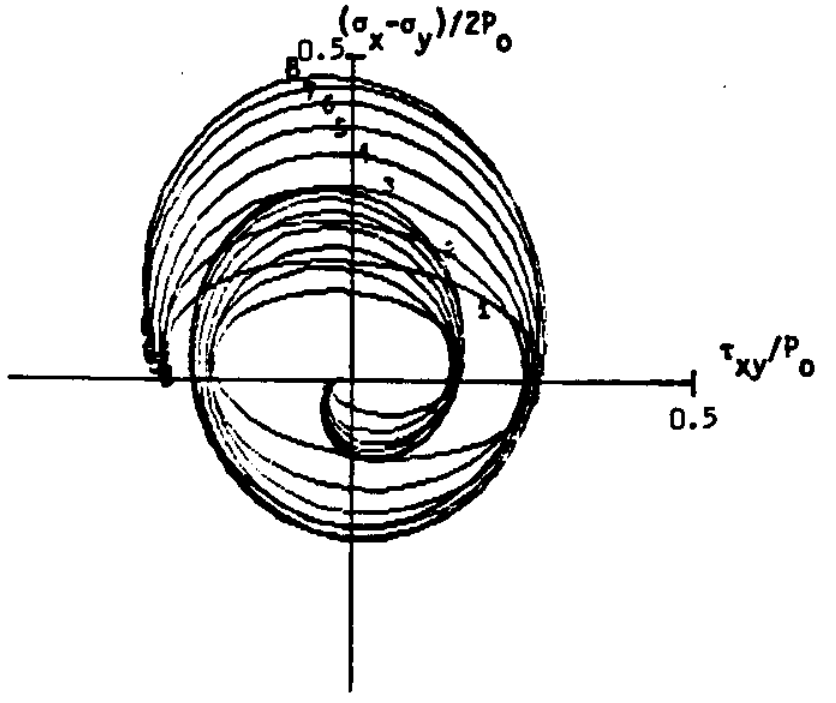

a) elements 1 to 8

b) elements 8 to 12

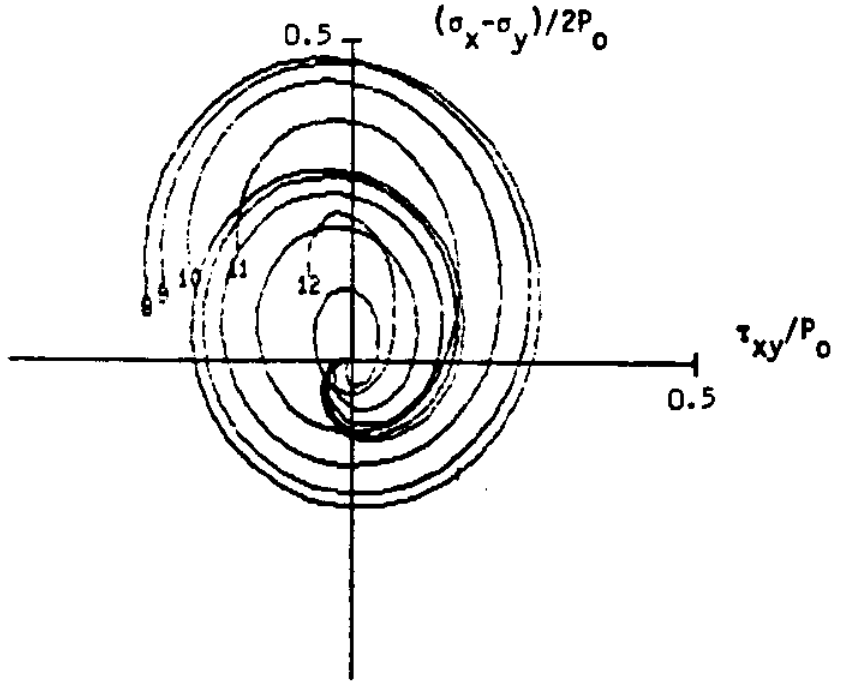

Fig. 17. Stress paths in the wave tank deposit

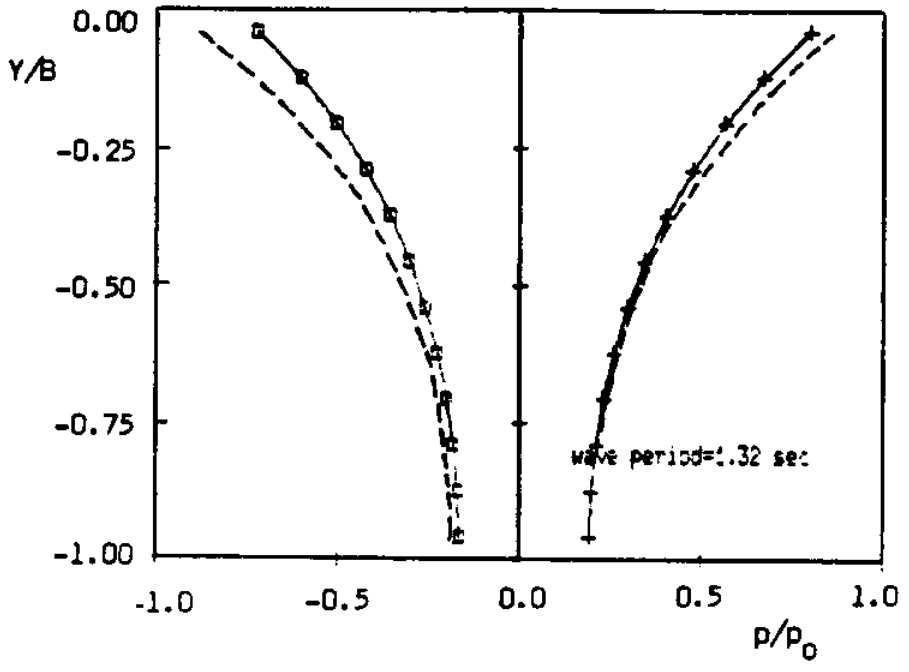

a) pore water pressure p vs depth y

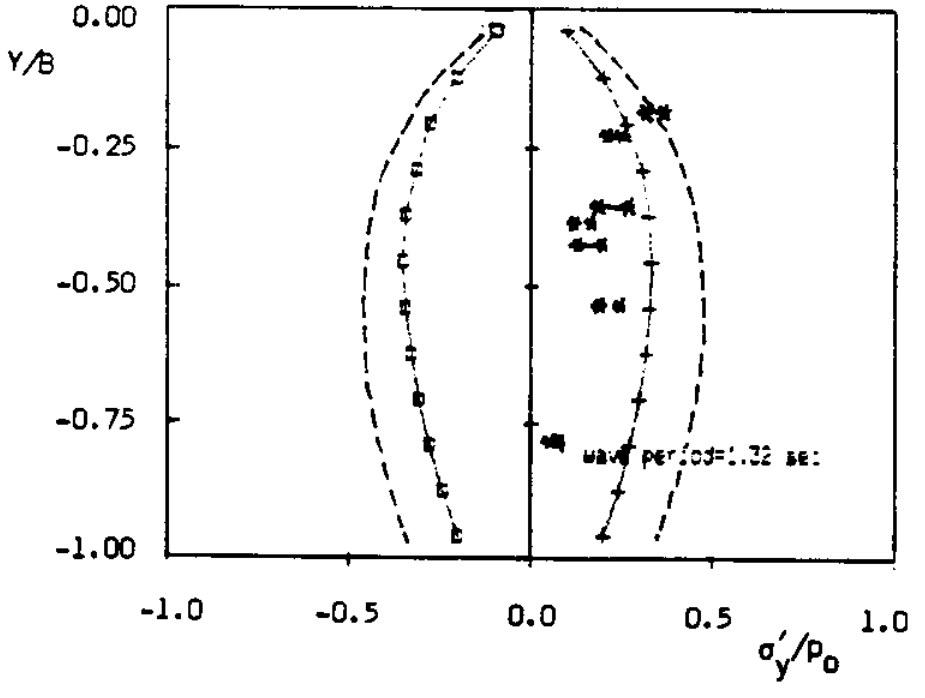

b) vertical effective stress σ_y vs depth y

Fig. 18. Amplitudes of stresses in the wave tank deposit
----- elastic solution ——— elastoplastic solution
**** experiment points (from (3))

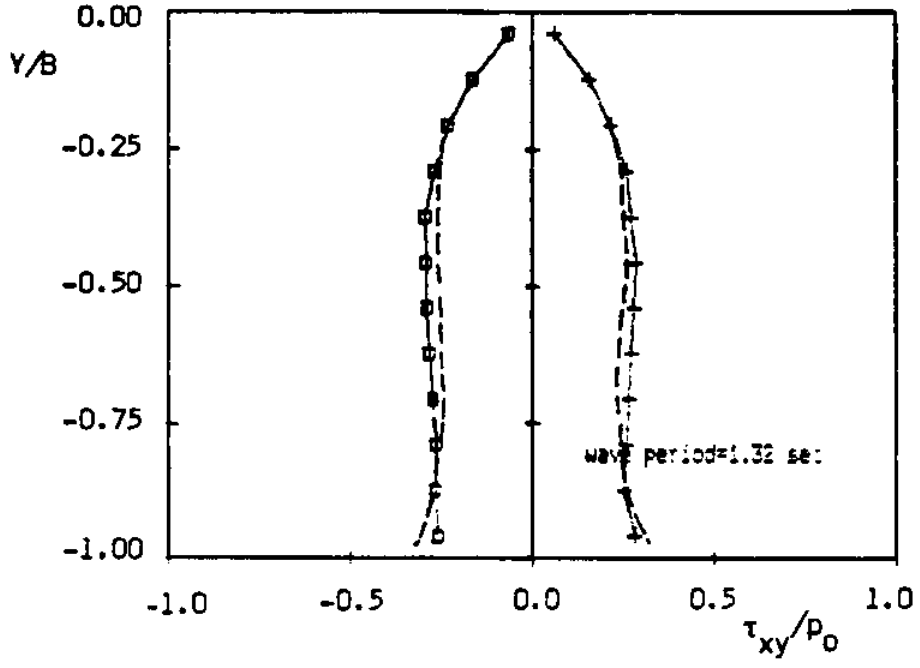

18.c) shear stress τ_{xy} vs depth y

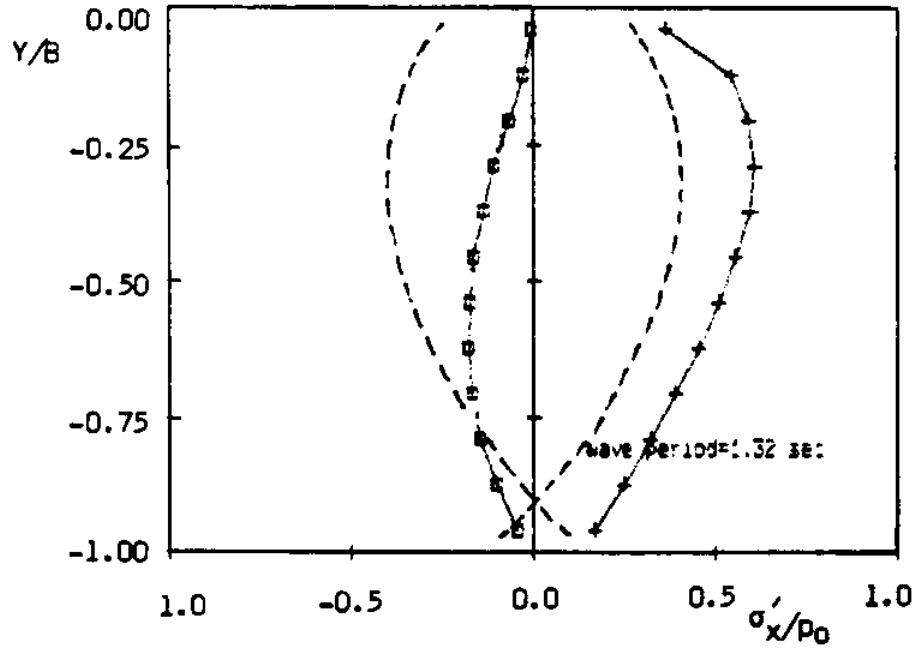

18.d) horizontal effective stress σ'_x vs depth y

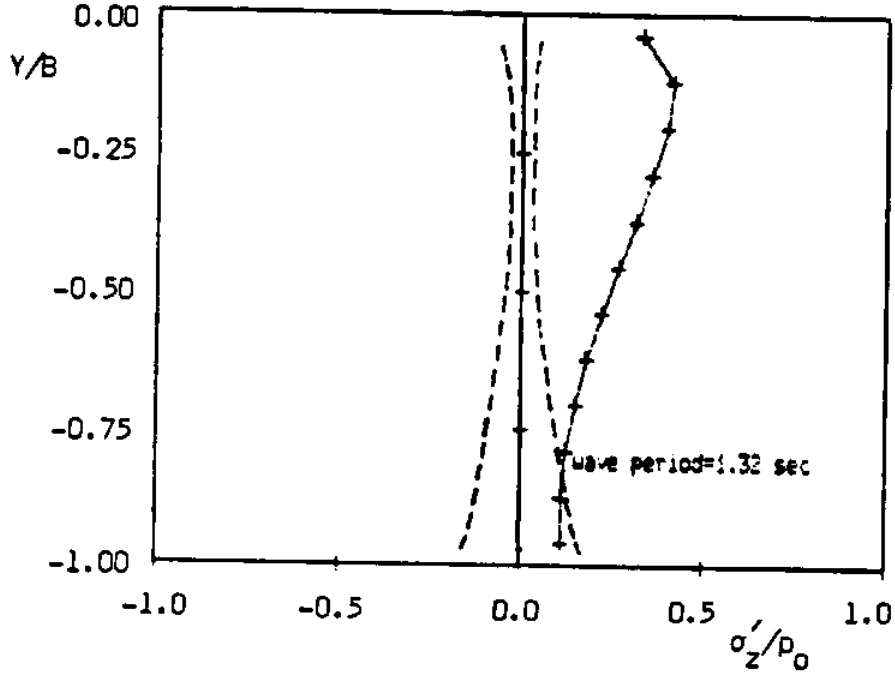

18.e) lateral effective stress σ_z' vs depth y

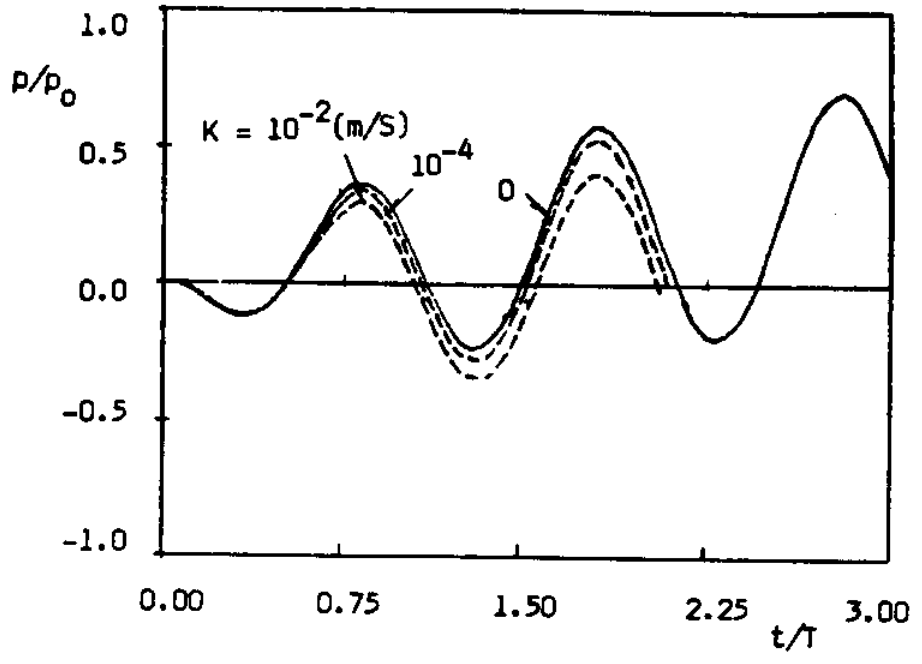

a) pore water pressure

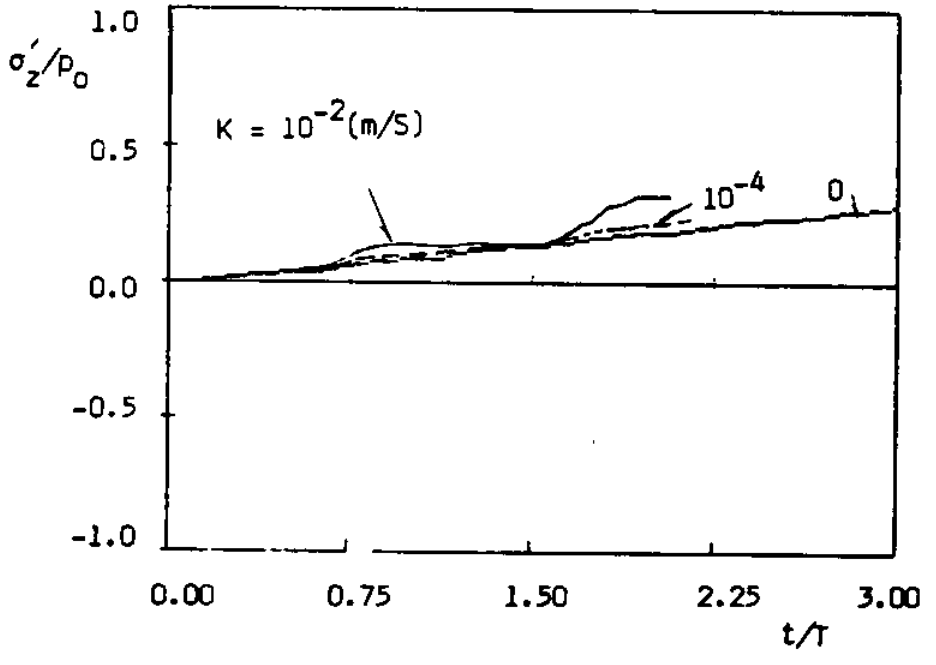

b) lateral effective stress σ'_z

Fig. 19. Time history of stresses in the wave tank deposit

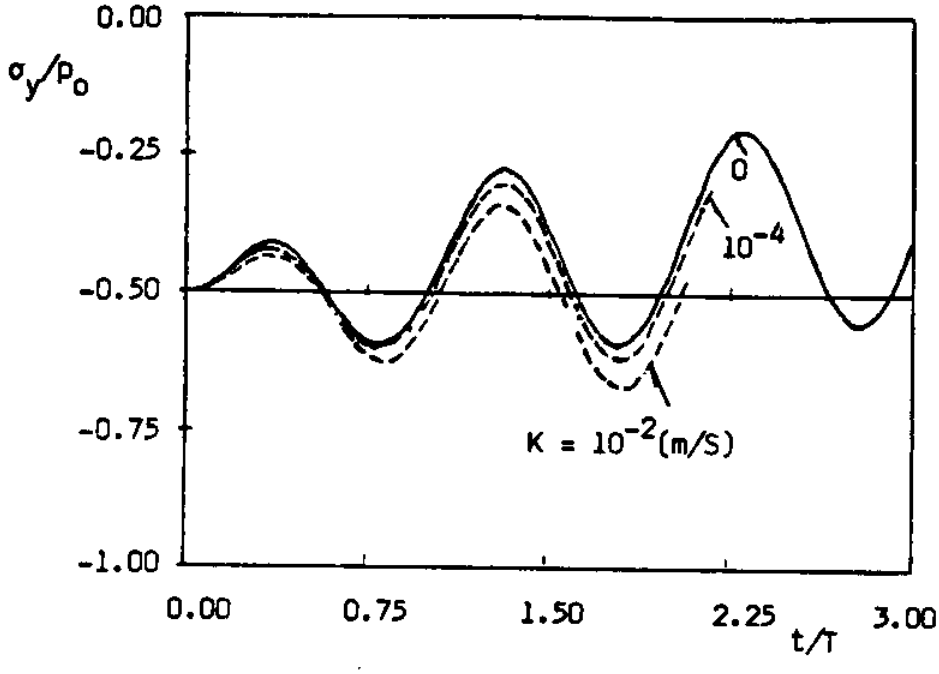

19.c) vertical effective stress σ_y

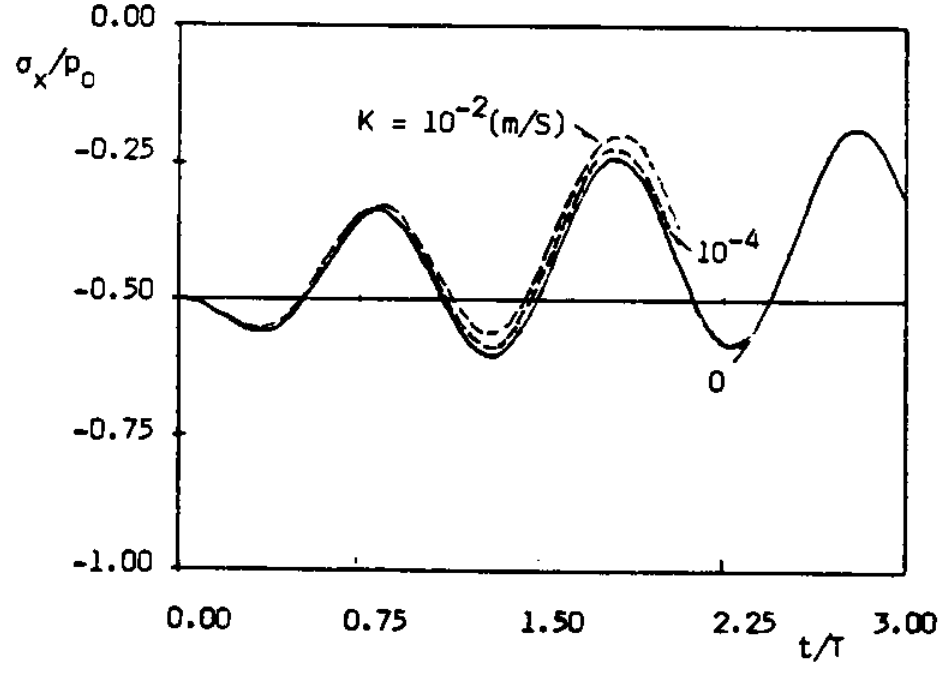

19.d) horizontal effective stress σ_x

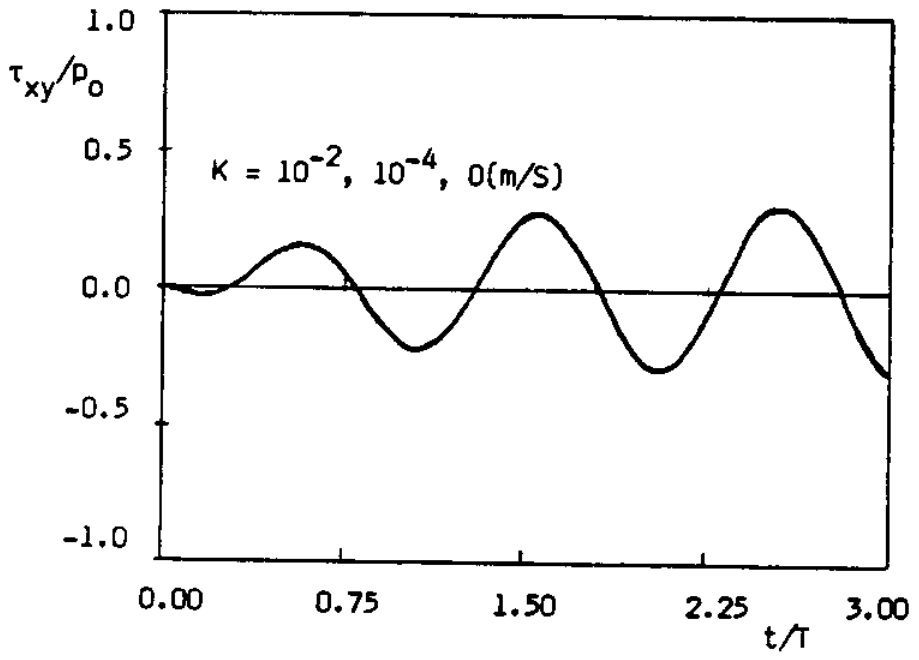

19.e) shear stress τ_{xy}

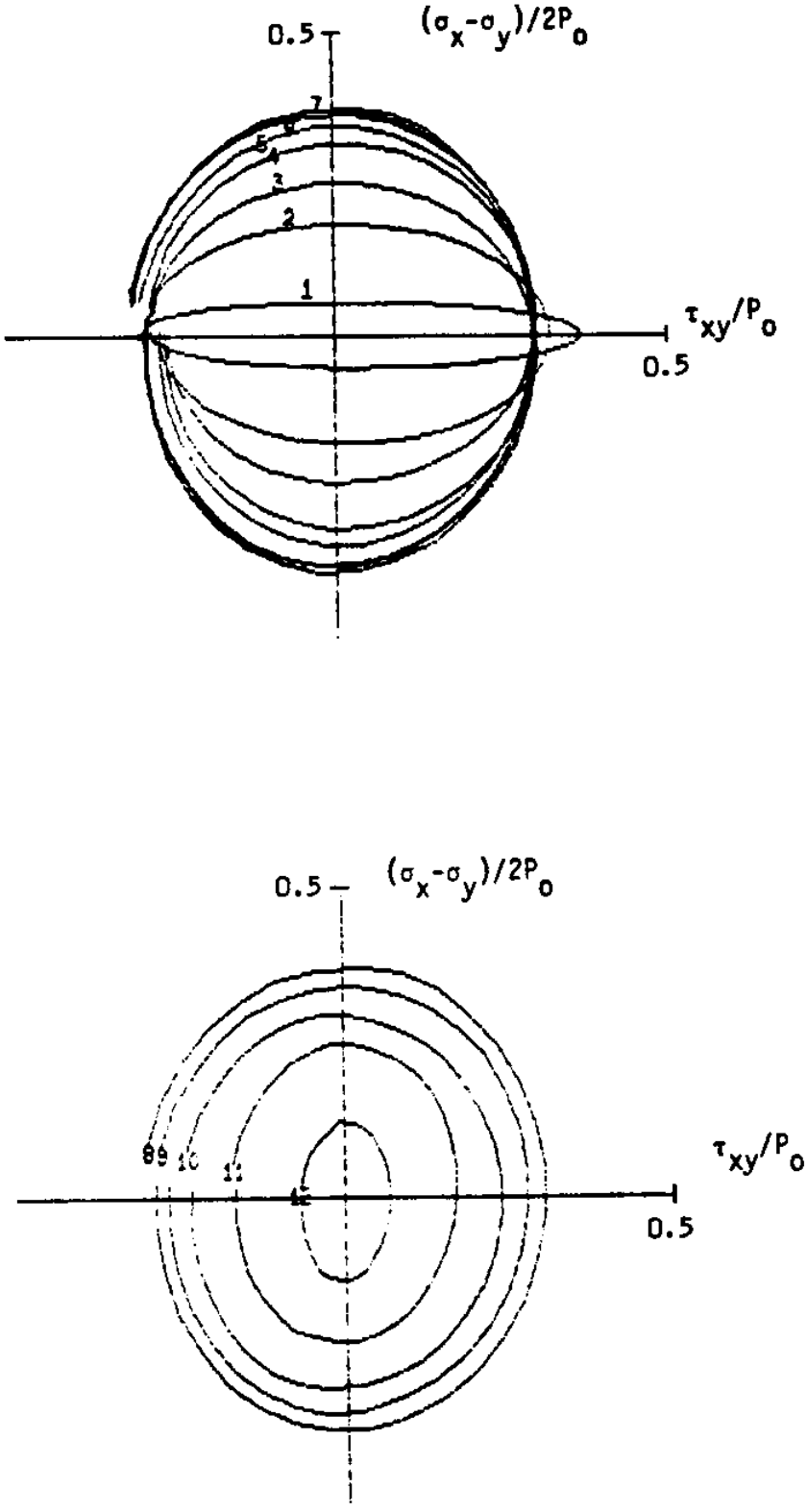

Fig. 20. Stress paths of the wave tank deposit under undrained condition (k = 0.0)